Tensor decomposition enhanced LRFS multi-DOA tracking based on coprime array

Tao Liang
School of Information and Communication Engineering, University of Electronic Science and Technology of China, Chengdu, China

Lin Gao, Senior Member, IEEE
School of Information and Communication Engineering, University of Electronic Science and Technology of China, Chengdu, China

Liangliang Li
School of Information and Communication Engineering, University of Electronic Science and Technology of China, Chengdu, China

Chaoqun Yang, Senior Member, IEEE
School of Automation, Southeast University, Nanjing, China

Ting Yuan, Senior Member, IEEE
School of Automation and Intelligent Sensing, Shanghai Jiao Tong University, Shanghai, China

Yuxuan Xia, Member, IEEE
School of Automation and Intelligent Sensing, Shanghai Jiao Tong University, Shanghai, China

Ping Wei
School of Information and Communication Engineering, University of Electronic Science and Technology of China, Chengdu, China

***Abstract*— This paper addresses the problem of tracking a time-varying number of multiple direction-of-arrival (multi-DOA) by exploiting the received signals of a coprime array. The multi-DOA state is represented by a labeled random finite set (LRFS), which is further modeled using the generalized labeled multi-Bernoulli (GLMB) distribution. Therefore, the GLMB filter naturally arises as a suitable method to propagate the multi-DOA posterior, from which the multi-DOA state can be extracted. To capture the intrinsic high dimensional characteristics of the signals received by the coprime array, a tensor model is adopted, followed by the canonical polyadic decomposition (CPD) to extract the rank-1 components of the tensor, which contain the spatial information corresponding to each source. Building on such a result, we formulate the multi-DOA likelihood in the form of a von Mises–Fisher (vMF) distribution. This likelihood enables the derivation of the update equation for the GLMB filter.Furthermore, we developed a particle-based implementation of the algorithm, and its effectiveness is subsequently assessed through simulation experiments. Even under low SNR and limited snapshot conditions, the proposed algorithm can accurately track the multi-DOA of time-varying source numbers, with the generalized optimal subpattern assignment (GOSPA) error remaining within $0.5°$.**

***Index Terms*— Multi-DOA tracking, canonical polyadic decomposition, labeled random finite sets, GLMB filter, von Mises-Fisher distribution.**

I. INTRODUCTION

Estimating the direction-of-arrival (DOA) is a core problem in array signal processing and underpins many applications, including non-cooperative sensing [1], radar [2], sonar [3], wireless communications [4], and acoustic source localization [5]. Over recent decades, a variety of high-resolution techniques have been proposed for DOA estimation. These range from subspace-based methods, such as multiple signal classification (MUSIC) [6] and estimation of signal parameters via rotational invariance techniques (ESPRIT) [7], to sparse-reconstruction approaches built on compressed sensing (CS) theory [8], [9] However, MUSIC and ESPRIT algorithms require accurate covariance estimation from signal samples, together with prior information on the number of sources. These requirements reduce their effectiveness when operating in low signal-to-noise ratio (SNR) environments or with few available snapshots. Although CS algorithms relax the requirement of knowing in advance the number of existing sources, they introduce other issues, such as grid mismatch, high computational complexity, and sensitivity to the sparsity assumption. Apart from these methods, many studies have explored multi-DOA tracking from received signals [10]–[15], but they typically assume predetermined and constant source number, limiting their applicability in scenarios where the sources number varies over time. As a result, these DOA estimation and tracking algorithms are unsuitable for scenarios with a time-varying number of sources.

The framework of random finite sets (RFS) [16] offers a rigorous Bayesian methodology for handling multi-target filtering, accommodating variations in both the number of targets and the state of each target over time. Representative filters developed under the RFS paradigm include the probability hypothesis density (PHD) filter [17], cardinalized PHD (CPHD) [18], the multi-Bernoulli (MB) filter [19], the Poisson multi-Bernoulli mixture (PMBM) filter [20], [21], and labeled RFS (LRFS)-based approaches such as the generalized labeled multi-Bernoulli (GLMB) [22]–[24] and the labeled multi-Bernoulli (LMB) filters [25]. The LRFS framework [22], [23] offers a natural way to directly estimate target trajectories. In the case of the GLMB filter [22], the labeled multi-target posterior is precisely updated, ensuring that

This work was supported by the National Natural Science Foundation of China under grant No. 62471110. Corresponding author: L. Gao.

T. Liang, L. Gao, L. Li and P. Wei are with the School of Information and Communication Engineering, University of Electronic Science and Technology of China, Chengdu, China. Emails: liangtao_uestc@126.com, lingao_1014@126.com, liliangliang_uestc@126.com, pwei@uestc.edu.cn.
C. Yang is with the School of Automation, Southeast University, Nanjing, Jiangsu, China. E-mail: ycq@seu.edu.cn.
T. Yuan and Y. Xia are with the School of Automation and Intelligent Sensing, Shanghai Jiao Tong University, Shanghai, China. Emails: tyuan@sjtu.edu.cn, yuxuan.xia@sjtu.edu.cn.

full information on target states and their association history is retained. Though this approach yields an accurate posterior representation, it also incurs a considerably greater computational burden than the LMB filter [25], which acts as an efficient approximation to the GLMB. Both filters inherently provide labeled estimates, enabling straightforward trajectory extraction. In order to leverage this advantage, our work employs the LRFS framework for the multi-DOA tracking problem.

In the application of multi-DOA tracking with RFS-based filters, traditional methods typically extract DOA measurements via algorithms such as MUSIC or ESPRIT, then use them to perform multi-target filters. However, such approaches discard the statistical properties inherent in the raw array measurements and introduce errors during the measurement extraction process, which limits tracking performance. In reality, the received signals follow a superpositional measurement model, i.e., the observations represent a coherent sum of contributions from multiple sources. Though RFS/LRFS-based algorithms have been developed for superpositional measurements, including exact and approximate PHD/CPHD filters [26]–[29], MB filters [30], and GLMB/LMB filters [31]–[34], these methods cannot be directly applied to DOA tracking. This is because existing superpositional measurement models assume deterministic amplitude-based signals. These models are incompatible with DOA scenarios, where source amplitudes are modeled as random processes with zero mean, and the DOA information is embedded in the phase differences among the elements of the array. Additionally, directly modeling these randomly fluctuating source signals in an augmented state formulation can be cumbersome due to the high dimensionality. A CPHD-based multi-DOA tracking approach was proposed in [35], which directly processes the covariance matrix rather than the raw signals. However, its performance is limited since the CPHD filter is an approximate Bayesian multi-target filter. In [36], a new measurement association mapping (NMAP) method has been proposed by building an association pseudo-likelihood based on the MUSIC spectrum, which in turn facilitates employing particle GLMB filter for multi-DOA tracking. Besides, the distributed multi-DOA tracking problem has been considered, and a wireless sensor network based PHD algorithm for DOA tracking has been proposed in [37].

The aforementioned studies primarily focus on uniform linear arrays (ULAs), which, however, require a large number of physical sensors to achieve high resolution, resulting in increased hardware cost, power consumption, and system complexity. Recently, sparse arrays have gained increasing attention for achieving high resolution and accurate estimation with fewer physical sensors by extending the virtual aperture, among which coprime arrays represent a prominent design formed by interleaving two uniform subarrays defined by coprime integers [38]. However, research on multi-DOA tracking with coprime arrays remains limited, mainly due to the challenges posed by the sparse and non-uniform virtual array structure, which creates difficulties in constructing reliable association and likelihood models. Recent works such as [39] and [40] have investigated multi-DOA tracking on coprime arrays by employing the exponentially weighted MUSIC pseudo-spectrum as a measurement likelihood, thereby enabling the application of particle implementations of PHD and GLMB filters.

This paper addresses multi-DOA tracking utilizing coprime arrays, which, for a given number of sensors, provide a larger virtual array aperture than ULAs, resulting in improved estimation performance. Due to the fact that signals received by coprime arrays have intrinsic high dimensional relationships, a spatial covariance tensor is constructed from multiple snapshots data segments, and the canonical polyadic decomposition (CPD) is employed to derive the rank-1 components of the tensor which, contains the steering vector information of sources. The resulting steering vectors lie on the unit hypersphere, and therefore they can be naturally modeled using the von Mises-Fisher (vMF) distribution, which is characterized by its concentration parameter. This likelihood is subsequently incorporated into a robust GLMB filter that operates in environments with uncertain detection probabilities and background clutter, enabling the joint estimation of both the varying number of sources over time and their corresponding trajectories.

It is worth pointing out that, in the NMAP-based multi-DOA tracking algorithm [40], a similar construction strategy for likelihood has been carried out by exploiting singular value decomposition (SVD), and the rank-1 approximation was implemented based on the leading singular vector. Such SVD results in the reconstructed covariance matrix, based on which one can get a pseudo-likelihood that contains data association between the pseudo-spectrum and DOAs. However, it does not ensure a strict one-to-one mapping between the reconstructed covariance matrix and individual source, and is prone to multi-peak artifacts in the pseudo-spectrum, particularly under low SNR or closely spaced DOA conditions. In contrast, leveraging the uniqueness of CPD, this paper constructs a strict one-to-one mapping between the decomposed steering vector measurements and the sources, resulting in more principled likelihoods and improved tracking robustness. More importantly, the multi-DOA tracker adopted by [40] relies on explicit and accurate detection probabilities and clutter intensity, which are actually intractable in most of DOA tracking scenarios. Compared to the heuristic pseudo-likelihood of NMAP, the vMF likelihood proposed in this paper enables seamless integration with standard clutter models within the RFS framework, facilitating the construction of a mathematically consistent multi-target likelihood. The key contributions of this paper are presented below:

- Derivation of a CPD model that represents the spatial covariance tensor from multiple snapshots data segments.

- Proposal of a vMF based likelihood for multi-DOA tracking based on a coprime array.
- Developments of a robust GLMB filter for multi-DOA tracking based on a coprime array.

The rest of this paper is arranged as follows. Section II introduces the notations appeared throughout this paper. Section III provides background material relevant to GLMB-based multi-DOA tracking. Section IV presents details of proposed algorithm. Numerical experiments are discussed in Section V, with final conclusions given in Section VI.

II. Notations

Scalars, vectors, matrices, tensors, and sets are represented by lowercase letters (e.g., a), bold lowercase letters (e.g., $\mathbf{a}$), bold uppercase letters (e.g., $\mathbf{A}$), bold calligraphic letters (e.g., $\boldsymbol{\mathcal{A}}$), and calligraphic letters (e.g., $\mathcal{A}$), respectively. The unfolding of a tensor $\boldsymbol{\mathcal{A}}$ along mode-n is expressed as $\mathbf{A}_{(n)}$. Blackboard bold symbols (e.g., $\mathbb{L}$) indicate spaces, where $\mathbb{R}$ and $\mathbb{C}$ stand for the sets of real and complex numbers, respectively. For a set $\mathcal{A}$, its cardinality is written as $|\mathcal{A}|$. The notations $(\cdot)^\top$, $(\cdot)^*$, and $(\cdot)^H$ refer to the transpose, the complex conjugate, and the Hermitian (conjugate transpose), respectively. The Frobenius norm of a matrix is given by $\|\cdot\|_F$, while $\|\cdot\|_2$ denotes the Euclidean (or ℓ_2) norm of a vector. The symbol $\mathbf{I}_n$ denotes the $n \times n$ identity matrix. A real Gaussian distribution with mean μ and variance σ^2 is denoted as $\mathcal{N}(\cdot; \mu, \sigma^2)$. The operations $\circ$, $\otimes$, and $\odot$ stand for the outer product, the Kronecker product, and the Khatri–Rao product (i.e., column-wise Kronecker product), respectively.

III. Background

A. Problem formulation

In this paper, the problem of coprime array based multi-DOA tracking in scenarios where the number of sources varies over time is considered. It is assumed that there are Q_k far-field narrowband sources $s_{i,k}, i \in \{1, \cdots, Q_k\}$ impinging on a coprime array at time k with DOAs denoted by $\theta_{i,k}$ for $i \in \{1, 2, \ldots, Q_k\}$. Based on the received signal by the coprime array, the goal is to develop a recursive framework that jointly estimates the time-varying source number and DOAs while ensuring reliable target association and continuous trajectory tracking over time. To begin with, we first introduce the concept of the coprime array together with the corresponding signal model. The preliminaries relevant to the proposed algorithm are followed in the subsequent subsections, including the outline of GLMB filtering recursion, tensor representation and CPD.

A coprime array is composed of two ULAs, i.e., one with N_1 elements spaced $(2N_2 - 1)d$, and the other with N_2 elements spaced $(N_1 - 1)d$. Here, N_1 and N_2 are assumed to be coprime integers, and without loss of generality, we take $N_1 > N_2$. The inter-element distance is set to $d = \lambda/2$, where λ denotes the signal wavelength. Due to the inherent properties of coprime integers, if the first element of one array is chosen as the reference, the remaining elements are positioned such that no overlap occurs when the two ULAs are aligned. The element locations can be expressed as a set given by

$$\begin{aligned}\mathcal{P} = &\{pdN_1 \mid p \in \{0, \ldots, 2N_2 - 1\}\} \\ &\cup \{qdN_2 \mid q \in \{0, \ldots, N_1 - 1\}\}. \end{aligned} \tag{1}$$

Then the sampled signal vector $\mathbf{y}_k \in \mathbb{C}^{(N_1+N_2-1)\times 1}$ is given by

$$\mathbf{y}_k = \sum_{i=1}^{Q_k} \mathbf{a}(\theta_{i,k}) s_{i,k} + \mathbf{v}_k, \tag{2}$$

where $\mathbf{v}_k$ denotes the zero-mean Gaussian measurement noise with covariance $\sigma^2 \mathbf{I}_{N_2+N_1-1}$. The steering vector $\mathbf{a}(\theta_{i,k})$ is defined as

$$\mathbf{a}(\theta_{i,k}) = \left[1, \cdots, e^{-j\frac{2\pi}{\lambda} n_p \sin(\theta_{i,k})}\right]^\top, \tag{3}$$

with $n_p \in \mathcal{P}$ being the array location indices. It should be noted that, due to the fact that the array output results from the superposition of multiple source signals arriving at the array, model (2) is often referred to as a superpositional measurement model [35].

Since the signal waveforms are unknown and difficult to process directly, conventional array signal processing techniques typically exploit their second-order statistics. The covariance matrix $\mathbf{R}_k$ associated with $\mathbf{y}_k$ in (2) can be expressed as

$$\mathbf{R}_k = \mathbb{E}(\mathbf{y}_k \mathbf{y}_k^H) = \sum_{i=1}^{Q_k} \sigma_i^2 \mathbf{a}(\theta_{i,k}) \mathbf{a}(\theta_{i,k})^H + \sigma^2 \mathbf{I}_{N_2+N_1-1}, \tag{4}$$

where $\mathbb{E}(\cdot)$ denotes the expectation operator, and σ_i^2 denotes the i-th source power. In practice, the covariance matrix is obtained using a limited set of snapshots. Specifically, we collect J samples at time k into a data matrix as

$$\mathbf{Y}_k = \left[\mathbf{y}_k, \mathbf{y}_{k+T_s}, \cdots, \mathbf{y}_{k+(J-1)T_s}\right], \tag{5}$$

where T_s denotes the sampling period. Here we assume $k + JT_s \ll k+1$, which can generally be satisfied since T_s should be a very small number so as to satisfy Nyquist's sampling condition. The measurement model can then be rewritten as

$$\mathbf{Y}_k = \mathbf{A}(\boldsymbol{\theta}) \mathbf{S}_k + \mathbf{V}_k, \tag{6}$$

where $\mathbf{A}(\boldsymbol{\theta}) = [\mathbf{a}(\theta_{1,k}), \ldots, \mathbf{a}(\theta_{Q_k,k})]$ is the array manifold, $\mathbf{S}_k = [\mathbf{s}_{1,k}, \cdots, \mathbf{s}_{Q_k,k}]^\top$ with signal vector defined as $\mathbf{s}_{i,k} = \left[s_{i,k}, s_{i,k+T_s}, \cdots, s_{i,k+(J-1)T_s}\right]^\top$. Then the covariance matrix can be estimated using

$$\widehat{\mathbf{R}}_k = \mathbf{Y}_k \mathbf{Y}_k^H / J. \tag{7}$$

In coprime array processing [38], the sample covariance matrix is typically vectorized, and redundant terms are

removed to construct an extended virtual array data vector, which is expressed as

$$\mathbf{r}_k = \widetilde{\mathbf{A}}_k \mathbf{b}_k + \sigma^2 \mathbf{1}_{N_2N_1+N_2}, \tag{8}$$

where $\widetilde{\mathbf{A}}_k = [\widetilde{\mathbf{a}}(\theta_{1,k}), \ldots, \widetilde{\mathbf{a}}(\theta_{Q_k,k})]$ represents the array manifold of a virtual ULA comprising $2N_2(N_1+1)-1$ elements, with positions ranging from $(-N_2(N_1+1)+1)d$ to $(N_2(N_1+1)-1)d$, the vector $\mathbf{b}_k = \left[\sigma_1^2, \ldots, \sigma_{Q_k}^2\right]^\top$ specifies the source powers, and $\mathbf{1}_{N_2N_1+N_2} \in \mathbb{R}^{(2N_2(N_1+1)-1)\times 1}$ denotes a unit vector whose only nonzero entry is located at index $(N_2N_1+N_2)$. Due to the fact that $\mathbf{r}_k$ corresponds to a single-snapshot measurement vector of the virtual array, its outer product produces a covariance matrix with rank deficiency, reducing the effectiveness of subspace-based DOA estimation methods. To overcome this limitation, a spatial smoothing approach [41] is applied to recover the rank. Specifically, $\mathbf{r}_k$ is divided into $M = N_2(N_1+1)$ overlapping sub-vectors $\{\mathbf{r}_{j,k}\}_{j=1}^{M}$. These sub-vectors are then used to compute the spatially smoothed covariance matrix as

$$\widetilde{\mathbf{R}}_k = \frac{1}{M}\sum_{j=1}^{M} \mathbf{r}_{j,k}\mathbf{r}_{j,k}^H, \tag{9}$$

where $\mathbf{r}_{j,k}$ represents a sub-vector of $\mathbf{r}_k$ starting from the j-th entry and ending at the $(M+j-1)$-th entry, with $M = N_2(N_1+1)$ denoting the total number of smoothing subarrays. The resulting full-rank matrix $\widetilde{\mathbf{R}}_k$ allows for the efficient application of subspace-based DOA estimation techniques, such as MUSIC.

Based on the above formulations, it can be seen that $\widetilde{\mathbf{R}}_k$ is constructed from the received signals of each element in the coprime array. The received signals are contributed by Q_k sources, where Q_k is not known a priori by the multi-DOA tracking algorithm. In this paper, we model the multi-DOA distribution with the GLMB density, where each potential source is attached by a unique label. As far as GLMB distribution is obtained, the probability mass function of the source number can be exactly computed according to [23, Sec. VI-A], based on which the maximum a posterior (MAP) or expected a posterior (EAP) criterion can be employed to obtain the estimate of Q_k. The details of GLMB distribution are introduced in the subsequent Section III-B. **[P1.13]** Overall, this problem can be summarized as the recursive estimation of the time-varying source number Q_k and the tracking of their DOAs $\theta_{i,k}$, $i \in \{1, \ldots, Q_k\}$, using the smoothed covariance matrix $\widetilde{\mathbf{R}}_k$ in (9).

B. Outline of the GLMB filter

Following the same definition as in [40], the state of a single source is defined as $\mathbf{x}_k = [\theta_k, \dot{\theta}_k]^\top$, where $\theta_k, \dot{\theta}_k$ denote the DOA and the change rate of the DOA at time k, respectively. The rationale for including $\dot{\theta}_k$ inside the source state is that, for a given time interval Δ_T, by assuming that the source undergoes smooth motion, the source DOA at time k can be reasonably predicted by the dynamic model (details are provided in (52)). Such a prediction is necessary for the GLMB filter (actually the prediction step is necessary for any Bayesian filter), so as to synchronize the prior knowledge with the measurements. In this paper, the detection probability of source corresponding to each DOA is considered unknown, therefore we incorporate it into the state vector and define a new state as

$$\overline{\mathbf{x}}_k = [\mathbf{x}_k, \beta_k],$$

where β_k denotes the unknown detection probability of state $\mathbf{x}_k$. Since the number of sources Q_k generally varies over time, we introduce the LRFS $\mathcal{X}_k$ to represent the multiple-source state at time k, allowing the cardinality and the state of each element changing dynamically. Specifically, $\mathcal{X}_k$ is defined as

$$\mathcal{X}_k \triangleq \{(\overline{\mathbf{x}}_k^1, l_k^1), \ldots, (\overline{\mathbf{x}}_k^{N_k}, l_k^{N_k})\}, \tag{10}$$

where $\overline{\mathbf{x}}_k^i$ and l_k^i (for $i \in \{1, \ldots, N_k\}$) denote the state and artificially attached label of the i-th source, respectively. For ease of expression, we also denote $\beta(l)$ as the detection probability of source labeled by l without leading to any confusion. Although the label is not directly available, it is introduced to uniquely identify sources across time and to enable the reconstruction of individual source trajectories.

To describe the recursion of the GLMB filter, we define the measurement set at time k as

$$\mathcal{Z}_k \triangleq \{\mathbf{z}_k^1, \cdots, \mathbf{z}_k^{P_k}\}, \tag{11}$$

which consists of P_k elements, where $\mathbf{z}_k^p$ (for $p \in \{1, \ldots, P_k\}$) is specified as the steering vector of a potential source (see Section IV-A for details). This specification can be naturally handled by the GLMB filter described in this section. The multi-DOA Bayesian filter aims to recursively compute the posterior $\pi_k(\mathcal{X}|\mathcal{Z}_{1:k})$ (where $\mathcal{Z}_{1:k} \triangleq [\mathcal{Z}_1, \ldots, \mathcal{Z}_k]$), given the prior $\pi_{k-1}(\mathcal{X}|\mathcal{Z}_{1:k-1})$ and likelihood $g_k(\mathcal{Z}_k|\mathcal{X})$, which are detailed as

$$\pi_{k|k-1}(\mathcal{X}|\mathcal{Z}_{1:k-1}) = \int f_{k|k-1}(\mathcal{X}|\mathcal{U})\pi_{k-1}(\mathcal{U}|\mathcal{Z}_{1:k-1})\delta\mathcal{U}, \tag{12}$$

$$\pi_k(\mathcal{X}|\mathcal{Z}_{1:k}) = \frac{g_k(\mathcal{Z}_k|\mathcal{X})\pi_{k|k-1}(\mathcal{X}|\mathcal{Z}_{1:k-1})}{\int g_k(\mathcal{Z}_k|\mathcal{V})\pi_{k|k-1}(\mathcal{V}|\mathcal{Z}_{1:k-1})\delta\mathcal{V}}, \tag{13}$$

where $\int \cdot \delta\mathcal{X}$ denotes set integral with respect to the LRFS $\mathcal{X}$, $f_{k|k-1}$ is the multi-DOA transition density, and g_k is the multi-DOA likelihood function.

According to the finite set statistics [42], an LRFS state can be uniquely described by its multi-DOA distribution. In this paper, the GLMB distribution [22] is adopted to model the LRFS state. Specifically, recall the LRFS state $\mathcal{X}_k = \{(\overline{\mathbf{x}}_k^1, l_k^1), \ldots, (\overline{\mathbf{x}}_k^N, l_k^N)\}$, we define $I = \{l_k^1, \ldots, l_k^N\}$ as the corresponding label set, and we also define the mapping from $\mathcal{X}_k$ to I as $I = \mathcal{L}(\mathcal{X}_k)$. Although the GLMB is a closed-form multi-DOA density, its exact implementation is computationally intractable.

The GLMB distribution at time k is defined as [23]

$$\pi_k(\mathcal{X}) = \delta_{|\mathcal{X}|}(|\mathcal{L}(\mathcal{X})|) \sum_{(I,\xi)\subseteq\mathcal{F}(\mathbb{L}_k)\times\Xi} \delta_I(\mathcal{L}(\mathcal{X}))\omega_k^{I,\xi}\left[p_k^{\xi}\right]^{\mathcal{X}}, \quad (14)$$

where:

- $\delta_{|\mathcal{X}|}(|\mathcal{L}(\mathcal{X})|)$ equals 1 only when $\mathcal{X}$ and its label set $\mathcal{L}(\mathcal{X})$ share the same cardinality. $\mathbb{L}_k$ denotes the label space of the GLMB distribution, which may vary over time due to target births and deaths. $\mathcal{F}(\mathbb{L}_k)$ denotes the collection of all finite subsets of $\mathbb{L}_k$.
- The association mapping function from label set to measurements, i.e., $\phi : I \to \{0, 1, \ldots, |\mathcal{Z}_k|\}$ satisfying $\phi(l_k) = \phi(l'_k)$ and $\phi(l_k) > 0 \Rightarrow l_k = l'_k$, which ensures that each measurement is linked to no more than one label. Here, $\phi(l_k) = 0$ indicates a missed detection (i.e., no measurement is associated with label l_k), while $\phi(l_k) > 0$ means that the label l_k is associated with the measurement $\mathbf{z}_k^{\phi(l_k)}$. However, $\phi(l_k) = \phi(l'_k) = 0$ does not necessarily lead to $l_k = l'_k$. The collection of all such functions forms the association map space Φ. For a domain $I \subseteq \mathbb{L}$, the corresponding subset of association maps is denoted by $\Phi(I)$.
- The discrete index set Ξ represents the collection of all association map histories up to time k, given by $\Phi_{0:k} \triangleq \Phi_0 \times \Phi_1 \times \cdots \times \Phi_k$. A pair (I, ξ) corresponds to a history measurement association (hypothesis), and $\omega_k^{I,\xi}$ denotes the weight assigned to the hypothesis with label set I, satisfying $\sum_{(I,\xi)\subseteq\mathcal{F}(\mathbb{L}_k)\times\Xi} \omega_k^{I,\xi} = 1$.
- $p_k^{\xi} \triangleq p_k^{\xi}(\overline{\mathbf{x}}, l)$ denotes the spatial probability density function (SPDF) with label $l \in \mathbb{L}_k$, and $[p]^{\mathcal{X}} \triangleq \prod_{\overline{\mathbf{x}}\in\mathcal{X}} p(\overline{\mathbf{x}}, l)$ is the multi-DOA exponential notation.

As it can be seen from (14) that the GLMB density can be uniquely defined by the weight and SPDF of all hypotheses, thus we abbreviate (14) by

$$\pi_k(\mathcal{X}) = \{\omega_k^{I,\xi}, p_k^{\xi}\}_{(I,\xi)\in\mathcal{F}(\mathbb{L})\times\Xi}. \quad (15)$$

Furthermore, we also have the birth GLMB density given by $\pi_k^B(\mathcal{X}) = \{\omega_k^{B,I}, p_k^B\}_{I\in\mathcal{F}(\mathbb{L}_B)}$.

For simplicity in notation, the subsequent derivations omit the time index k and label l. We set $\mathcal{X} \triangleq \mathcal{X}_k$, $\mathbb{L}_+ \triangleq \mathbb{L}_{0:k-1} \cup \mathbb{L}_{\mathbb{B}}$, $\pi_+(\mathcal{X}) \triangleq \pi_{k+1|k}(\mathcal{X})$, $g \triangleq g_k$, $f \triangleq f_{k+1|k}$, and $\mathcal{Z} \triangleq \mathcal{Z}_k$. Accordingly, the predicted GLMB density can be written as

$$\pi_+(\mathcal{X}) = \{\omega_+^{I_+,\xi}, p_+^{\xi}\}_{(I_+,\xi)\in\mathcal{F}(\mathbb{L}_+\times\Xi)}. \quad (16)$$

where the GLMB prediction step for obtaining it is omitted for brevity, see [23] for details. Substituting predicted density $\pi_+(\mathcal{X})$ into the Bayesian update equation (13), yields the GLMB posterior as follows

$$\pi(\mathcal{X}) = \{\omega^{I_+,\xi,\phi}, p^{\xi,\phi}\}_{(I_+,\xi)\in\mathcal{F}(\mathbb{L}_+\times\Xi),\phi\in\Phi(I_+)}. \quad (17)$$

where $\Phi(I_+)$ denotes the subsets of current association maps with labels set I_+,

$$\omega^{I_+,\xi,\phi} \propto \omega_+^{I_+,\xi} \prod_{l\in I_+} \eta^{\xi,\phi}(l), \quad (18)$$

$$\eta^{\xi,\phi}(l) = \int p^{\xi}(\overline{\mathbf{x}}, l)\psi(\overline{\mathbf{x}}, l; \phi)d\overline{\mathbf{x}}, \quad (19)$$

$$p^{\xi,\phi} \triangleq p^{\xi,\phi}(\overline{\mathbf{x}}, l|\mathcal{Z}) = \frac{p^{\xi}(\overline{\mathbf{x}}, l)\,\psi(\overline{\mathbf{x}}, l; \phi)}{\eta^{\xi,\phi}(l)}, l \in I_+, \quad (20)$$

$$\psi(\overline{\mathbf{x}}, l; \phi) = \begin{cases} \frac{\beta(l)g(\mathbf{z}^{\phi(l)}|\mathbf{x},l)}{\alpha(\mathbf{z}^{\phi(l)})}, & \phi(l) > 0 \\ 1 - \beta(l), & \phi(l) = 0 \end{cases}. \quad (21)$$

where ϕ denotes the current measurement association mapping function; $\beta(l)$ and $(\mathbf{x}, l)$ denote the detection probability and kinematic state (i.e., θ and $\dot{\theta}$) of label l; $g(\mathbf{z}^{\phi(l)}|\mathbf{x}, l)$ is the single-DOA likelihood function and $\alpha(\mathbf{z}^{\phi(l)})$ denotes the clutter likelihood.

C. Tensor and CPD preliminaries

Tensors extend the concept of vectors and matrices to represent data in higher-order forms. Typically, an N-th order tensor can be described as a multi-dimensional array indexed by N modes. To keep the notations clear, tensors are expressed using bold calligraphic symbols (e.g., $\boldsymbol{\mathcal{Y}}$), with subscripts indicating their individual elements. As an example, let $\boldsymbol{\mathcal{Y}} \in \mathbb{R}^{U\times V\times W}$ be a third-order tensor. Its entries are denoted by $\boldsymbol{\mathcal{Y}}_{u,v,w}$, with $u = 1, \ldots, U$, $v = 1, \ldots, V$, and $w = 1, \ldots, W$. In this paper, the CPD of a third-tensor will be exploited in deriving the proposed likelihood, so we give some related definitions as follows.

DEFINITION 1 *Let $\mathbf{m} \in \mathbb{C}^U$ and $\mathbf{n} \in \mathbb{C}^V$ be two vectors. Their outer product is an $U \times V$ matrix whose (u, v)-th entry is given by*

$$(\mathbf{m} \circ \mathbf{n})_{u,v} = \mathbf{m}(u)\,\mathbf{n}(v), \quad u = 1, \ldots, U,\ v = 1, \ldots, V.$$

More generally, for $\mathbf{m} \in \mathbb{C}^U$, $\mathbf{n} \in \mathbb{C}^V$, and $\mathbf{p} \in \mathbb{C}^W$, their outer product forms a third-order tensor $\boldsymbol{\mathcal{Y}} \in \mathbb{C}^{U\times V\times W}$, with each element expressed as $\boldsymbol{\mathcal{Y}}_{u,v,w} = \mathbf{m}(u)\,\mathbf{n}(v)\,\mathbf{p}(w)$.

DEFINITION 2 *A third-order tensor $\boldsymbol{\mathcal{Y}} \in \mathbb{C}^{U\times V\times W}$ is of rank-1 if it can be expressed as the outer product of three vectors. In other words, there exist $\mathbf{m} \in \mathbb{C}^U$, $\mathbf{n} \in \mathbb{C}^V$, and $\mathbf{p} \in \mathbb{C}^W$ such that*

$$\boldsymbol{\mathcal{Y}}_{u,v,w} = \mathbf{m}(u)\,\mathbf{n}(v)\,\mathbf{p}(w), \quad \text{for all } u, v, w.$$

DEFINITION 3 *For a third-order tensor $\boldsymbol{\mathcal{Y}} \in \mathbb{C}^{U\times V\times W}$, its rank is the smallest integer $R > 0$ such that it can be decomposed into a sum of R rank-1 tensors, i.e.,*

$$\boldsymbol{\mathcal{Y}} = \sum_{r=1}^{R} \mathbf{m}_r \circ \mathbf{n}_r \circ \mathbf{p}_r, \quad (22)$$

where $\mathbf{m}_r \in \mathbb{C}^U$, $\mathbf{n}_r \in \mathbb{C}^V$, and $\mathbf{p}_r \in \mathbb{C}^W$ for $r = 1, \ldots, R$, and the operator $\circ$ denotes the vector outer product. Throughout this paper, we also compactly rewrite the CPD (22) as

$$\boldsymbol{\mathcal{Y}} = [\![\mathbf{M}, \mathbf{N}, \mathbf{P}]\!], \quad (23)$$

with factor matrices $\mathbf{M} \triangleq [\mathbf{m}_1, \ldots, \mathbf{m}_R] \in \mathbb{C}^{U\times R}$, $\mathbf{N} \triangleq [\mathbf{n}_1, \ldots, \mathbf{n}_R] \in \mathbb{P}^{V\times R}$, and $\mathbf{C} \triangleq [\mathbf{p}_1, \ldots, \mathbf{p}_R] \in \mathbb{C}^{W\times R}$.

An important property of the CPD is its essential uniqueness. Specifically, the decomposition $\boldsymbol{\mathcal{Y}} =$

$[\![\mathbf{M},\mathbf{N},\mathbf{P}]\!]$ is essentially unique if, for any alternative decomposition $\boldsymbol{\mathcal{Y}} = [\![\overline{\mathbf{M}},\overline{\mathbf{N}},\overline{\mathbf{P}}]\!]$, there exists a permutation matrix $\boldsymbol{\Pi}$ and invertible diagonal matrices $\boldsymbol{\Lambda}_1$, $\boldsymbol{\Lambda}_2$, and $\boldsymbol{\Lambda}_3$ such that

$$\overline{\mathbf{M}} = \mathbf{M}\boldsymbol{\Pi}\boldsymbol{\Lambda}_1, \quad \overline{\mathbf{N}} = \mathbf{N}\boldsymbol{\Pi}\boldsymbol{\Lambda}_2, \quad \overline{\mathbf{P}} = \mathbf{P}\boldsymbol{\Pi}\boldsymbol{\Lambda}_3, \tag{24}$$

with the constraint $\boldsymbol{\Lambda}_1\boldsymbol{\Lambda}_2\boldsymbol{\Lambda}_3 = \mathbf{I}$. Conditions under which this essential uniqueness holds have been thoroughly investigated; see, e.g., Kruskal's condition and its subsequent extensions [43] for further details. The CPD can also be written in matrix format, whose definition is given as follows.

DEFINITION 4 *Let $\boldsymbol{\mathcal{Y}} = [\![\mathbf{M},\mathbf{N},\mathbf{P}]\!] \in \mathbb{C}^{U\times V\times W}$ be a third-order tensor with rank-R CPD. The three mode-n unfoldings (matricizations) of $\boldsymbol{\mathcal{Y}}$ are given by [43]:*

$$\mathbf{Y}_{(1)} = (\mathbf{P}\odot\mathbf{N})\,\mathbf{M}^\top \in \mathbb{C}^{VW\times U}, \tag{25}$$
$$\mathbf{Y}_{(2)} = (\mathbf{P}\odot\mathbf{M})\,\mathbf{N}^\top \in \mathbb{C}^{UW\times V}, \tag{26}$$
$$\mathbf{Y}_{(3)} = (\mathbf{N}\odot\mathbf{M})\,\mathbf{P}^\top \in \mathbb{C}^{UV\times W}, \tag{27}$$

where $\odot$ denotes the Khatri–Rao product.

IV. The proposed multi-DOA tracking algorithm

A. Steering vector as measurement by CPD

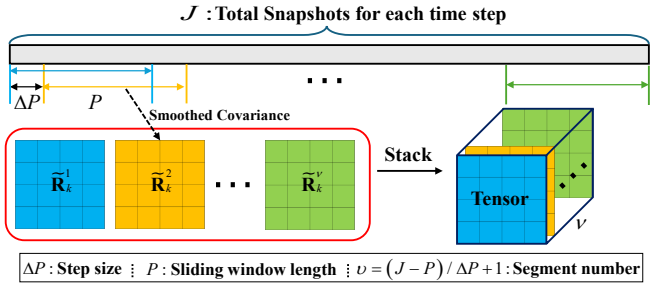

Fig. 1: The illustration of the tensor model for received signal by coprime array

As shown in Fig. 1, at each time step a sliding window of length P is applied to the J snapshots with step size ΔP, yielding $\nu = (J-P)/\Delta P + 1$ segmented snapshot sets. For each segmented snapshot set, a smoothed covariance matrix is constructed as given in Eq. (9). These smoothed covariance matrices are then stacked to form a tensor. In order to derive the proposed likelihood for multi-DOA tracking, it is convenient to reveal the intrinsic relationship between the smoothed covariance matrix (9) with the tensor model, as shown by the following proposition.

PROPOSITION 1 *Given ν segments of sampled data, we can obtain ν smoothed covariance matrices by (9). By stacking these matrices along the third dimension, $\boldsymbol{\mathcal{R}}_k(:,:,\gamma) = \widetilde{\mathbf{R}}_k^\gamma, \gamma = 1,\cdots,\nu$, the resulting multi-dimensional data can be regarded as a tensor admitting CPD, given by*

$$\boldsymbol{\mathcal{R}}_k \triangleq [\![\overline{\mathbf{A}}_k^*, \overline{\mathbf{A}}_k, \overline{\mathbf{D}}_k]\!] + \boldsymbol{\mathcal{U}}_k$$
$$= \sum_{i=1}^{Q_k} \overline{\mathbf{a}}^*(\theta_{i,k}) \circ \overline{\mathbf{a}}(\theta_{i,k}) \circ \overline{\mathbf{d}}_{i,k} + \boldsymbol{\mathcal{U}}_k, \tag{28}$$

where $*$ is the complex conjugate symbol, factors matrixs $\overline{\mathbf{A}}_k \triangleq [\overline{\mathbf{a}}(\theta_{1,k}),\cdots,\overline{\mathbf{a}}(\theta_{Q_k,k})]$ and $\overline{\mathbf{D}}_k \triangleq [\overline{\mathbf{d}}_{1,k},\cdots,\overline{\mathbf{d}}_{Q_k,k}]$ with

$$\overline{\mathbf{a}}(\theta_{i,k}) = \left[1,\cdots,e^{-j\frac{2\pi}{\lambda}(G-1)\sin(\theta_{i,k})}\right]^\top, \tag{29}$$
$$\overline{\mathbf{d}}_{i,k} = [\sigma_{i,1,k}^4,\ldots,\sigma_{i,\nu,k}^4]^T, \tag{30}$$

for $i = 1,\ldots,Q_k$, and $\boldsymbol{\mathcal{U}}_k$ accounts for noise contributions due to measurement noise and the finite sample data.

Proof: see Appendix A. ■

In the proposed CPD-based signal model, both $\overline{\mathbf{A}}_k^*$ and $\overline{\mathbf{A}}_k$ are constrained to lie in the Vandermonde space, while $\overline{\mathbf{D}}_k$ is required to be nonnegative. Accordingly, the CPD in (28) can be addressed by formulating it as a structured optimization framework:

$$\mathrm{CPD}(\boldsymbol{\mathcal{R}}_k) \triangleq \min_{\overline{\mathbf{A}}_k,\overline{\mathbf{D}}_k} \left\|\boldsymbol{\mathcal{R}}_k - [\![\overline{\mathbf{A}}_k^*, \overline{\mathbf{A}}_k, \overline{\mathbf{D}}_k]\!]\right\|_F^2 + r(\overline{\mathbf{D}}_k), \tag{31}$$

where $\|\cdot\|_F$ denotes the Frobenius norm, $\overline{\mathbf{A}}_k \in \mathcal{V}_\theta$ (with $\mathcal{V}_\theta$ being the Vandermonde manifold), and

$$r(\overline{\mathbf{D}}_k) = \begin{cases} 0, & \overline{\mathbf{D}}_k \geq 0, \\ \infty, & \text{otherwise.} \end{cases}$$

enforces the nonnegativity constraint on the third factor matrix. In general, the optimization problem described above is NP-hard and non-convex. A typical strategy to cope with this issue is to adopt an alternating optimization scheme [44], in which variables are updated one at a time while keeping the others fixed, and $\overline{\mathbf{D}}_k$ can be updated efficiently via a proximity operator. The implementation details are referred to [45]. Besides, to preserve the Vandermonde structure of $\overline{\mathbf{A}}_k$ during the optimization, the method proposed in [46] can be employed to ensure that the estimated factor matrices remain within the Vandermonde manifold. In addition, as determining the rank of a tensor is an NP-hard task, we adopt the minimum description length (MDL) criterion [47] to estimate the number of rank-1 components, denoted as P_k.

After performing CPD for the tensor $\boldsymbol{\mathcal{R}}_k$, we obtain the estimated factor matrices $\widehat{\mathbf{A}}_k$, defined as follows

$$\widehat{\mathbf{A}}_k \leftarrow \mathrm{CPD}(\boldsymbol{\mathcal{R}}_k). \tag{32}$$

As a result, the matrix $\widehat{\mathbf{A}}_k$ contains P_k estimated steering vectors, each corresponding to one potential source. These steering vectors are regarded as measurements and used as input to the proposed GLMB filter. Specifically, the p-th measurement $\mathbf{z}_k^p$ in the set $\mathcal{Z}_k$ (11) is defined as

$$\mathbf{z}_k^p = \frac{\widehat{\mathbf{a}}_{p,k}}{\|\widehat{\mathbf{a}}_{p,k}\|_2}, \quad p = 1,\ldots,P_k, \tag{33}$$

where $\widehat{\mathbf{a}}_{p,k}$ denotes the p-th column of $\widehat{\mathbf{A}}_k$.

B. Complex von Mises–Fisher likelihood

According to (28), steering vectors of potential sources are extracted via CPD. Due to the inherent scale ambiguity of CPD, the extracted steering vectors are normalized to have unit norm, yielding measurements defined in (33) that lie on the complex unit hypersphere $\mathbb{CS}^{M-1}$. In practice, these steering vectors are perturbed by noise (28), resulting in angular dispersion around the true normalized steering vector $\mathbf{a}/\sqrt{M} \in \mathbb{CS}^{M-1}$. Since both $\widehat{\mathbf{a}}$ and $\mathbf{a}/\sqrt{M}$ are unit-norm vectors in $\mathbb{C}^M$, the measurement error is constrained to the complex unit hypersphere $\mathbb{CS}^{M-1}$, and is inherently directional in nature.

To properly model this directional uncertainty, we adopt the complex vMF distribution, which is the maximum entropy distribution on the unit hypersphere given a mean direction and concentration parameter, making it a principled choice for modeling noisy unit-norm vectors. Therefore, we have the likelihood of single source related steering vector shown by the following proposition.

PROPOSITION 2 *Assume $\mathbf{z}_k^p$ is produced by source $(\mathbf{x}, l) \in \mathcal{X}$, then the corresponding single source likelihood has the form of vMF, i.e.,*

$$g(\mathbf{z}_k^p \mid \mathbf{x}, l) = C_M(\kappa) \exp\left(\frac{\kappa}{\sqrt{M}} \mathbf{a}(\mathbf{c}\mathbf{x}_i^{\xi})^H \widehat{\mathbf{a}}_{\phi(l)}\right), \quad (34)$$

where $\mathbf{a}(\cdot)$ is the predicted steering vector given the DOA; $\mathbf{c} \triangleq [1\ 0]$ extracts the DOA parameter from the kinematic state $\mathbf{x}$; the concentration parameter $\kappa \geq 0$; $C_M(\kappa)$ is the normalization constant given by

$$C_M(\kappa) = \frac{\kappa^{M-1}}{\pi^M I_{M-1}(\kappa)}, \quad (35)$$

with $I_{M-1}(\cdot)$ denoting the modified Bessel function of the first kind and order $M-1$.

■

It is worth noting that the likelihood associated with an individual source plays a crucial role in the update stage of the GLMB filter (17). Clearly (21) will be specified by (34) in the proposed algorithm. Besides, we have detection probability $\beta(l)$ incorporated into the source state, and thus it can be naturally plugin (21) based on the particle implementation that will be introduced later.

However, the clutter rate $\alpha(\cdot)$ in (21) also remains needed to be computed. In this paper, the clutter measurements are assumed to be uniformly distributed over the complex unit hypersphere $\mathbb{CS}^{M-1}$. The corresponding clutter likelihood function is given by

$$\alpha_c(\mathbf{z}) = \frac{\lambda_c}{S_d}, \quad (36)$$

where λ_c denotes the clutter rate, and S_d is the surface area of the $(M-1)$-dimensional complex unit sphere $\mathbb{CS}^{M-1}$, computed as

$$S_d = \frac{2\pi^M}{\Gamma(M)}, \quad (37)$$

with $\Gamma(\cdot)$ denoting the Gamma function. In this paper, we adopt the robust clutter rate estimation method proposed in [48], [49], where an auxiliary robust CPHD filter is run in parallel with the GLMB filter. At each time stage, the CPHD filter processes the same measurements and uses the predicted PHD and cardinality (derived from the GLMB density) to jointly model clutter and actual targets. The resulting clutter rate estimate is then fed back into the GLMB filter to refine its data association and target state estimation.

REMARK 1 *The difference between the vMF likelihood and the MUSIC pseudo-likelihood adopted in [40] lies in their modeling principles and statistical consistency. The MUSIC pseudo-likelihood is constructed heuristically by reconstructing a rank-one covariance matrix from the leading singular vectors obtained via SVD, followed by subspace decomposition to generate the pseudo-spectrum. This process, however, can lead to multi-peak artifacts and unreliable associations, especially under low SNR conditions where the subspace estimate becomes inaccurate. In contrast, the vMF likelihood provides a principled probabilistic model for the pseudo-measurements lying on the unit hypersphere, accurately characterizing directional uncertainty through its concentration parameter. This enables seamless integration with standard clutter models in RFS-based filters and supports mathematically consistent multi-DOA association.*

C. Implementation of CPD enhanced GLMB filtering for multi-DOA tracking

In this paper, we implement the proposed method using the sequential Monte Carlo (SMC) approach, due to the high non-linearity and non-Gaussian characteristics of the likelihood function in (34). Within the SMC framework, each predicted single-DOA SPDF $p_+^{\xi}(\overline{\mathbf{x}}, l)$ is approximated through a set of weighted particles, expressed as

$$p_+^{\xi}(\overline{\mathbf{x}}, l) = \left\{w_u^{\xi}(l),\ \overline{\mathbf{x}}_u^{\xi}(l)\right\}_{u=1}^{N_p}, \quad (38)$$

where N_p represents the number of particles, $w_u^{\xi}(l)$ denotes the weight assigned to the u-th particle, satisfying $\sum_{u=1}^{N_p} w_u^{\xi}(l) = 1$, and $\overline{\mathbf{x}}_u^{\xi}(l)$ denotes its state. With the particle representation (38), the GLMB density is uniquely determined by its set of hypotheses, their corresponding hypothesis weights, and the particle states and their weights. Specifically, the predicted GLMB density in (16) can be represented as

$$\pi_+(\mathcal{X}) = \left\{\left(I_+^h,\ \xi^h,\ \omega_+^h,\ \{w_u^h, \overline{\mathbf{x}}_u^h\}_{u=1}^{N_p}\right)\right\}_{h=1}^{H}, \quad (39)$$

where H denotes the number of global hypotheses, $\omega_+^h \triangleq \omega_+^{I_+^h, \xi^h}$, and $\{w_u^h, \overline{\mathbf{x}}_u^h\} \triangleq \{w_u^{\xi^h}(l), \overline{\mathbf{x}}_u^{\xi^h}(l)\}$, for $l \in I_+^h$.

Each predicted GLMB hypothesis (I_+, ξ) can generate a large number of new hypotheses (I_+, ξ, ϕ) when associated with the current set of measurements. Enumerating all new hypotheses is computationally intractable due to the combination explosion. A feasible strategy is to retain only the most significant ones, avoiding the exhaustive generation of all hypotheses and their corresponding

weights. This is achieved by formulating the update as a ranked assignment problem [23].

In particular, given a set of predicted tracks with label set $I_+ = \{l_1, \ldots, l_{|I_+|}\}$ and the current measurement set $\mathcal{Z}$ defined in (33) obtained via CPD (32). Each feasible association $\phi \in \Phi(I_+)$ can be described using a binary assignment matrix $\mathbf{S} \in \{0,1\}^{|I_+|\times|\mathcal{Z}|}$. Specifically, $S_{i,j} = 1$ holds exactly when track l_i is associated with the j-th measurement, i.e. $\phi(l_i) = j$, while each row and column sum is either 0 or 1. An all-zero i-th row corresponds to a missed detection of track l_i, while an all-zero j-th column corresponds to $\mathbf{z}^j$ being a false detection. The mapping from $\mathbf{S}$ to ϕ can thus be written as

$$\phi(l_i) = \sum_{j=1}^{|\mathcal{Z}|} j\, \delta_1(S_{i,j}), \quad i = 1, \ldots, |I_+|. \tag{40}$$

To formulate the assignment cost, we define the cost matrix $\mathbf{C}^{I_+,\xi} \in \mathbb{R}^{|I_+|\times|\mathcal{Z}|}$ as

$$\mathbf{C}^{I_+,\xi} = \begin{bmatrix} c_{1,1} & \cdots & c_{1,|\mathcal{Z}|} \\ \vdots & \ddots & \vdots \\ c_{|I_+|,1} & \cdots & c_{|I_+|,|\mathcal{Z}|} \end{bmatrix}, \tag{41}$$

where

$$c_{i,j} = -\ln \frac{\int p_+^{\xi}(\overline{\mathbf{x}}, l_i)\beta(l_i) g(\mathbf{z}^j \mid \mathbf{x}, l_i) d\overline{\mathbf{x}}}{\left(\int p_+^{\xi}(\overline{\mathbf{x}}, l_i)(1-\beta(l_i)) d\overline{\mathbf{x}}\right) \alpha(\mathbf{z}^j)}, \tag{42}$$

is the negative log-likelihood cost of assigning measurement $\mathbf{z}^j$ to track l_i. The optimal assignment $\mathbf{S}^*$ (and corresponding ϕ^*) is then obtained by minimizing the total cost $\mathrm{tr}\left((\mathbf{S}^*)^T \mathbf{C}^{(I_+,\xi)}\right)$ using, for example, the Hungarian algorithm [50] and Murty's algorithm [51].

REMARK 2 *Given each predicted hypothesis h, the number of new hypotheses generated by associating with the current measurement set is $|\Phi(I_+^h)|$, which grows combinatorially with $|I_+^h|$. To avoid exhaustively enumerating all these possibilities, the ranked assignment algorithm is employed to retain only the top T^h most probable associations under each hypothesis. Specifically, this truncation restricts attention to the T^h components with the largest weights, thereby ensuring tractable computation. A typical strategy is to set $T^h = \lceil \omega_+^h J_{\max} \rceil$ where $\lceil \cdot \rceil$ denotes the ceiling operator, yielding the smallest integer no less than the given value, and $J_{\max}$ is a predefined upper bound on the number of new hypotheses per predicted component.*

Moreover, the cost of a particular assignment $\mathbf{S}$ (and its corresponding ϕ) is directly related to the updated hypothesis weight via

$$\prod_{l\in I_+} \eta^{\xi,\phi}(l) = \exp\left(-\mathrm{tr}\left(\mathbf{S}^T \mathbf{C}^{(I_+,\xi)}\right)\right) \times \prod_{l\in I_+} \left(\int p_+^{\xi}(\overline{\mathbf{x}}, l)(1-\beta(l)) d\overline{\mathbf{x}}\right). \tag{43}$$

Hence, solving the ranked assignment also yields the updated hypothesis weight. The assignment cost $c_{i,j}$ can be evaluated numerically as

$$c_{i,j} = -\ln \frac{\sum_{u=1}^{N_p} w_u^{\xi}(l_i)\, \beta_u^{\xi}(l_i)\, g\left(\mathbf{z}^j | \mathbf{x}_u^{\xi}(l_i), l_i\right)}{\sum_{u=1}^{N_p} w_u^{\xi}(l_i) \left(1-\beta_u^{\xi}(l_i)\right) \alpha(\mathbf{z}^j)}. \tag{44}$$

Then, for a particular association history (ξ, ϕ), the likelihood computation (19) can be expressed in an alternative form as

$$\eta^{\xi,\phi}(l) = \sum_{u=1}^{N_p} w_u^{\xi}(l)\, \psi(\overline{\mathbf{x}}_u^{\xi}(l), l; \phi), \tag{45}$$

and the updated SPDF (20) can be approximated as a particle set:

$$p^{\xi,\phi}(\overline{\mathbf{x}}, l|\mathcal{Z}) = \left\{w_u^{\xi,\phi}(l),\, \overline{\mathbf{x}}_u^{\xi}(l)\right\}_{u=1}^{N_p}, \tag{46}$$

$$w_u^{\xi,\phi}(l) = \frac{\psi(\overline{\mathbf{x}}_u^{\xi}(l), l; \phi)\, w_u^{\xi}(l)}{\eta^{\xi,\phi}(l)}. \tag{47}$$

Based on the posterior GLMB, the multi-DOA state estimate can be computed in two steps. First, we determine the most probable cardinality by evaluating the cardinality distribution:

$$\rho(n) := \sum_{h=1}^{H} \sum_{j=1}^{T^h} \omega^{h,j}\, \delta_n\left(\left|I_+^{h,j}\right|\right), \quad n = 0, \ldots, N_{\max}, \tag{48}$$

where $N_{\max}$ is the maximum number of labels across all hypotheses. Applying the maximum a posteriori (MAP) principle, the estimate of the sources number turns out to be

$$\widehat{Q} = \arg\max_n \rho(n). \tag{49}$$

Next, the hypothesis with the highest weight among those with the estimated source number $\widehat{Q}$ is selected:

$$\widehat{h}, \widehat{j} := \arg\max_{h,j} \omega^{h,j} \delta_{\widehat{Q}}\left(|I_+^{h,j}|\right). \tag{50}$$

The final multi-DOA estimate $\widehat{\boldsymbol{\mathcal{X}}}$ is then formed by taking the mean of the posterior SPDF for each label:

$$\widehat{\boldsymbol{\mathcal{X}}} := \left\{(\overline{\mathbf{x}}, l) : l \in I_+^{\widehat{h},\widehat{j}}, \overline{\mathbf{x}} = \int \overline{\mathbf{x}}'\, p^{\widehat{h},\widehat{j}}(\overline{\mathbf{x}}', l)\, d\overline{\mathbf{x}}'\right\}. \tag{51}$$

The proposed multi-DOA tracking algorithm is concisely outlined in Algorithm 1.

V. Numerical results

In this paper, a nearly constant-velocity (NCV) dynamic model is adopted, where the evolution of the single-source state is governed by

$$\mathbf{x}_k = \mathbf{F}\mathbf{x}_{k-1} + \mathbf{D}\boldsymbol{\varpi}_k, \tag{52}$$

where $\boldsymbol{\varpi}_k$ is a normal Gaussian process, and

$$\mathbf{F} = \begin{bmatrix} 1 & \Delta_T \\ 0 & 1 \end{bmatrix}, \quad \mathbf{D} = \sigma_{\varpi}^2 \begin{bmatrix} \Delta_T^2/2 \\ \Delta_T \end{bmatrix}, \tag{53}$$

denote the transition matrix and, respectively, the process noise coefficient matrix, with Δ_T being the time interval. For detection probability, we assume it follows the following random-walk model, i.e.,

$$\beta_k = \beta_{k-1} + \varphi_k, \tag{54}$$

Algorithm 1 Proposed multi-DOA tracking algorithm

Input: $\left\{I_+^h,\ \xi^h,\ \omega_+^h,\ p_+^h\right\}_{h=1}^{H}$, $\mathbf{Y}$, $M, P, \Delta P, \nu, J_{\max}$.

Segment $\mathbf{Y}$ into ν overlapping windows of length P and step ΔP, i.e., $\{\mathbf{Y}^1, \mathbf{Y}^2, \ldots, \mathbf{Y}^\nu\}$;
for $i = 1 : \nu$ **do**
  Compute the covariance matrix $\widehat{\mathbf{R}}^i = \mathbf{Y}^i(\mathbf{Y}^i)^H/P$;
  Vectorize the covariance matrix and obtain $\mathbf{r}^i$ via (8);
  Recover full-rank covariance matrix $\widetilde{\mathbf{R}}^i$ via (9);
end for
Construct a third-order tensor by stacking the smoothed covariance: $\boldsymbol{\mathcal{R}}(:,:,i) = \widetilde{\mathbf{R}}^i, \quad i = 1, \ldots, \nu$;
Perform CPD for tensor $\boldsymbol{\mathcal{R}}$ and obtain a set of measurements $\mathcal{Z}$ via (32) and (33);
Perform robust CPHD recursion proposed in [48] and compute clutter rate λ_c from the posterior CPHD;
for $h = 1 : H$ **do**
  Compute the cost matrix $\mathbf{C}^h \triangleq \mathbf{C}^{I_+^h, \xi^h}$ by (41) and (44);
  Solve the *ranked-assignment*$(\mathcal{Z}, I_+^h, \mathbf{C}^h, T^h)$ problem and obtain $T^h = \omega_+^h J_{\max}$ most probable associations, i.e., $\{\phi^{h,j}\}_{j=1}^{T^h}$;
  for $j = 1$ **do**
    Compute $\eta^{h,j}(l) \triangleq \eta^{\xi^h, \phi^{h,j}}(l), l \in I_+$ by (45);
    Update density $p^{h,j} \triangleq p^{\xi^h, \phi^{h,j}}(\overline{\mathbf{x}}, l|\mathcal{Z})$ by (46) and (47) with VMF likelihood (34);
    Compute $\omega^{h,j}$ via (18);
    Let $I^{h,j} = I_+^h$ and $\xi^{h,j} = (\xi^h, \phi^{h,j})$;
  end for
end for
Normalize weights $\left\{\omega^{h,j}\right\}_{h\in H, j\in T^h}^{H,T^h}$;
Extract multi-DOA estimate $\widehat{\boldsymbol{\mathcal{X}}}$ via (48)–(51);

Output: $\widehat{\boldsymbol{\mathcal{X}}}$.

where φ_k is the zero-mean Gaussian process noise with covariance σ_φ^2. It is reasonable because the detection probability generally changes gradually over time, rather than experiencing abrupt jumps. Under this assumption, we effectively maintain the mean of the detection probability while increasing its uncertainty through noise with a certain variance. This is consistent with physical intuition, and a similar temporal evolution model has been adopted in [49]. In our simulations, we set the time step period $\Delta_T = 1s$ and Gaussian process noise with covariance $\sigma_\varpi^2 = 0.2°/s^2$ and $\sigma_\varphi^2 = 0.1$. It is assumed that a coprime array of $N_1 = 5, N_2 = 3$ equispaced omnidirectional antennas is deployed, where the inter-sensor spacing is set to be $d = 1.5m$, and the sampling frequency is $f_s = 200\text{MHz}$. The range of all DOAs is restricted to $[-90°, 90°]$. The SNR is defined as

$$\Gamma_{\text{SNR}} = 10\log_{10}\sigma_s^2/\sigma^2, \tag{55}$$

where σ_s^2 and σ^2 denote the signal power and noise power, respectively. In all simulations, the step size fo the sliding window is set as $\Delta P = 10$.

To better illustrate the performance of the proposed method, several simulation benchmarks are included for comparison, including the CPHD based multi-DOA tracking with superpositional model [35] (referred to CPHD-Super), the GLMB filter using the MUSIC pseudo-likelihood [40] (referred to GLMB-MUSIC), and the proposed method in ULA configuration with the same elements (Proposed-ULA). Although the CPHD-Super algorithm was originally developed for a ULA, its core is based on the statistical properties of the received signals. The algorithm assumes that the received signals can be modeled as Gaussian random vectors, with the sample covariance matrices following a complex Wishart distribution. This assumption remains valid for coprime arrays, allowing the CPHD-Super algorithm to be directly extended to coprime arrays. Thus, including the CPHD-Super algorithm as a benchmark is both fair and meaningful. The generalized optimal subpattern assignment (GOSPA) metric [52] with cut-off parameter $c = 3^o$, order $p = 2$, and $\alpha = 2$ is employed to evaluate the performance of the algorithms. All simulations were carried out using a desktop system equipped with a 2.90 GHz Intel i7-10700 CPU, 32 GB RAM, and running Windows 11 together with Matlab R2024a. All simulation results were averaged over 100 Monte Carlo trials.

REMARK 3 *The proposed algorithm differs from Proposed-ULA in the aspect that the coprime array is employed by the proposed method, while the Proposed-ULA employed a ULA which has the same number of antenna elements as the coprime array, leading to different DOA estimation and resolution abilities. The motivation for comparing the proposed method to Proposed-ULA is that, the main focus of this paper is to address the problem of multi-DOA tracking based on the coprime array, thus we also want to show the accuracy improvement by employing the coprime array compared to the ULA, which has been widely considered by many DOA estimation or tracking algorithms. It is worth noting that the ULA can be directly adopted by the proposed algorithm with only trivial modifications, due to the fact that the difference between coprime array and the ULA lies only in the different array element spacing, thus the proposed tensor model for the coprime array can be directly applied to the ULA by modifying the tensor as* $\boldsymbol{\mathcal{R}}_k(:,:,\gamma) = \mathbf{R}_k^\gamma, \gamma = 1, \cdots, \nu$ *where* $\mathbf{R}_k^\gamma = \frac{1}{P}\sum_{j=1}^{P}\mathbf{y}_{j,k}\mathbf{y}_{j,k}^H$ *denotes the sampling covariance matrix.*

A. Multi-DOA tracking with fixed source number scenario

This subsection considers a multi-DOA tracking scenario with three sources, each having the same survival time of 1-50s. The initial states of the sources are $\mathbf{x}^1 = [41.2, -1.2]^\top, \mathbf{x}^2 = [-45.6, 0.8]^\top$ and $\mathbf{x}^3 = [20.6, -0.2]^\top$.

Considering the algorithm related parameters, the LMB birth model $\boldsymbol{\pi}_B = \{r_B^i, p_B^i\}_{i=1}^3$ is adopted [23], where the existence probabilities are set as $r_B^1 = 0.02$, $r_B^2 = 0.03, r_B^3 = 0.02$, and the SPDFs of the birth components p_B^i are represented by $N_p = 100$ particles sampled from Gaussian distributions $\mathcal{N}(\mathbf{x}^i; \mathbf{m}^i, \mathbf{P})$ where the mean and covariance parameters are $\mathbf{m}^1 = [40, 0]^\top$, $\mathbf{m}^2 = [-45, 0]^\top$, $\mathbf{m}^3 = [20, 0]^\top$ and $\mathbf{P} = \text{diag}\left(2^2, 0\right)$. The initial detection probability of each birth source is sampled from a uniform distribution $\mathcal{U}_{[0.5,1]}(\beta)$. For particle propagation, we use the single-source transition density as the proposal distribution. After each update, resampling is performed when the effective number of particles $N_{\text{eff}} = 1/\sum_{j=1}^{N}(w_j)^2$ falls below a predefined threshold (typically $N_{\text{eff}} < 0.5N_p$) to mitigate particle degeneracy, and w_j denotes the normalized weight of the j-th particle.

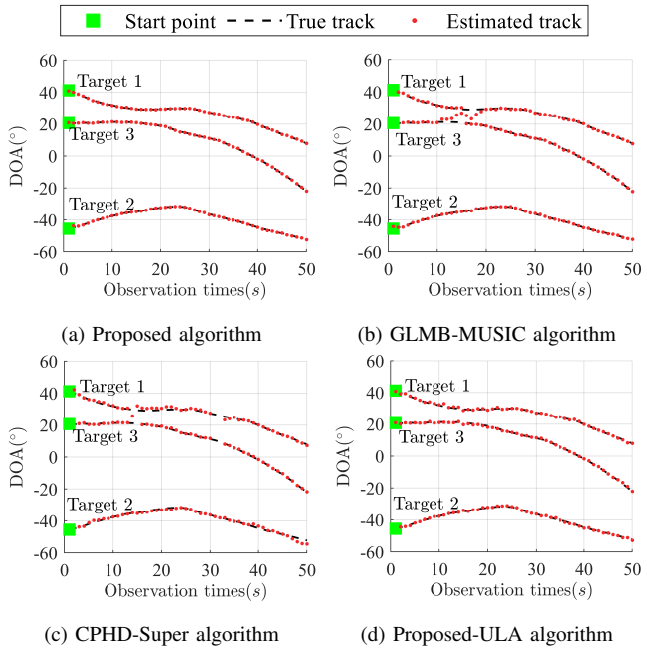

(a) Proposed algorithm (b) GLMB-MUSIC algorithm

(c) CPHD-Super algorithm (d) Proposed-ULA algorithm

Fig. 2: An example Monte Carlo trial under $\Gamma_{\text{SNR}} = -2\text{dB}, J = 200$ and $P = 100$

Figure 2 shows the tracking result for a representative trial, and it can be observed that the proposed algorithm outperforms the other algorithms. Specifically, the GLMB-MUSIC shows a significant performance degradation when the two DOAs are close to each other around time $10 - 20$s, but the tracking performance recovers as the DOAs gradually separate. Meanwhile, CPHD-Super suffers from missed detection, and the trajectory estimation of Proposed-ULA is notably worse than the proposed algorithm, which exhibits smoother trajectory estimation. Figures 3 and 4 show the GOSPA error and its decomposed three principal components, i.e., the estimation error for the correctly associated DOA, missed and false detection. As it is shown, the proposed algorithm exhibits the lowest estimation error throughout the observation period, with rarely any missed detection or false detection. Although Fig. 5 shows that GLMB-MUSIC accurately estimates the source number, Fig. 4 reveals missed detection and false detection around $10 - 20$s. This is due to the DOA estimation performance degraded when two DOAs are close, causing the DOA with large deviation to be considered false detection, which also results in missed detection. CPHD-Super exhibits the worst overall performance, being prone to missed detection after stable tracking periods and having lower estimation accuracy than the other algorithms. While the Proposed-ULA can reliably estimate the number of sources, its performance is inferior to that of the proposed algorithm, especially when the DOAs are close. Figure 6 compares the average GOSPA error (time-normalized results) of the involved algorithms under different SNR and snapshot conditions, which can be seen that the proposed algorithm consistently achieves the smallest error across all SNR and snapshot conditions. Even under low SNR (e.g., -6dB) and limited snapshots (e.g., $J = 60$), it maintains a GOSPA estimation error within $0.5°$. The Proposed-ULA performs worse than GLMB-MUSIC under the conditions of $\Gamma_{\text{SNR}} < -4\text{dB}$ and $J < 100$, indicating that the proposed algorithm is less robust to noise in the ULA compared to the coprime array. It is noted that the GOSPA error of GLMB-MUSIC does not show significant variation versus SNR and snapshots when $\Gamma_{\text{SNR}} > -6\text{dB}$, suggesting that the performance degradation when DOAs are close is not due to noise, but rather because the signal subspaces of adjacent sources are no longer well separated, causing the MUSIC-based pseudo-likelihood to deteriorate.

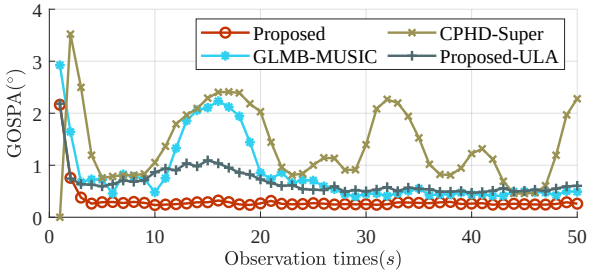

Fig. 3: GOSPA errors under $\Gamma_{\text{SNR}} = -2\text{dB}, J = 200$ and $P = 100$

B. Multi-DOA tracking with time-varying source number scenario

To further verify the effectiveness of the proposed algorithm in the time-varying source number scenario, this subsection considers tracking the DOAs of 5 narrowband sources, and the survival time of each source summarized in Table I. The LMB birth model $\boldsymbol{\pi}_B = \{r_B^i, p_B^i\}_{i=1}^4$ is adopted, with existence probabilities set as $r_B^1 = 0.02$, $r_B^2 = 0.03$, $r_B^3 = 0.02$, and $r_B^4 = 0.02$. The SPDFs of the birth components are represented by $N_p = 100$ particles sampled from Gaussian distributions $\mathcal{N}(\mathbf{x}; \mathbf{m}, \mathbf{P})$ where

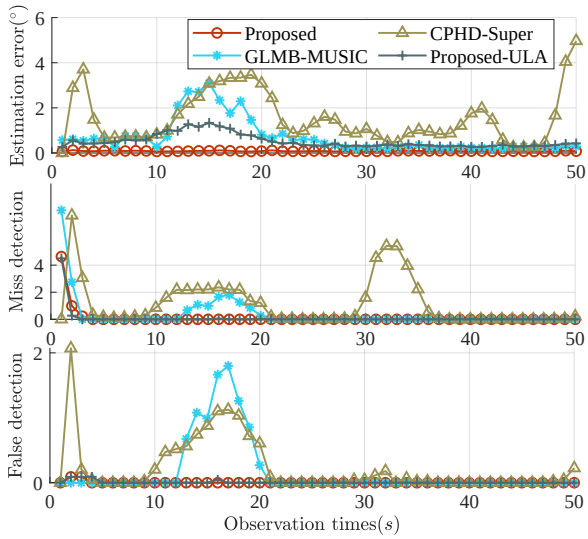

Fig. 4: DOA estimation error, missed and false detection errors under $\Gamma_{\text{SNR}} = -2\text{dB}$, $J = 200$ and $P = 100$

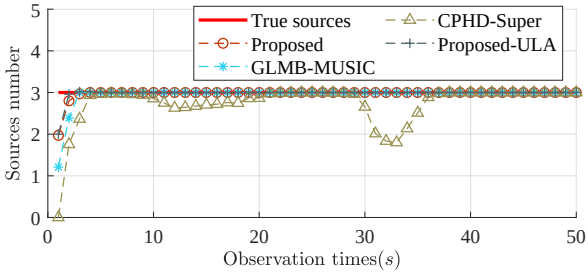

Fig. 5: Source number estimation under $\Gamma_{\text{SNR}} = -2\text{dB}$, $J = 200$ and $P = 100$

mean and covariance parameters are detailed in Table II. All other conditions are consistent with the fixed source scenario.

The tracking results for a representative trial are shown in Fig. 7, which qualitatively demonstrate that the proposed algorithm outperforms the other compared methods. In particular, during the two DOA crossing periods (10–12s for Targets 1–2 and 63–66s for Targets 4–5), the proposed algorithm and Proposed–ULA maintain track continuity and precise estimation, whereas GLMB–MUSIC exhibits noticeable estimation errors and CPHD–Super suffers from missed detection. These phenomena are further quantitatively reflected in Figs. 8–10. In Fig. 8, it can be observed that the GLMB–MUSIC produces noticeable source number estimation errors when the number of sources changes (i.e., during source appearance or disappearance). In contrast, the CPHD–Super exhibits severe missed detection under the same condition and requires a long period after the DOAs separate to recover accurate tracking, as highlighted by the blue dashed circle in Fig. 7(c). Compared with the proposed algorithm, the Proposed–ULA is less robust, being more prone to missed detection when the DOAs are closely spaced, and exhibits lower tracking accuracy, as clearly shown in the zoomed-in regions of Figs. 7(a) and 7(d). This performance gap arises from the larger virtual aperture of the coprime array, which offers enhanced angular resolution and estimation precision. Figure 9 illustrates the evolution of the overall GOSPA error over time. It can be seen that the proposed algorithm consistently achieves the lowest overall error throughout the tracking period. The peaks in the GOSPA curves correspond to moments when the number of sources changes or when DOAs become closely spaced. In these challenging scenarios, the proposed algorithm demonstrates strong robustness and maintains minimal estimation error, whereas the other three algorithms exhibit sharp error spikes, with CPHD–Super showing the largest errors, followed by GLMB–MUSIC and Proposed–ULA. Figure 10 further

TABLE I: Source survival state

Source	Survival time(s)	Initial DOA (degree)	Velocities (rad/s)
1	1–40	31.2	-1.2
2	6–50	10	1
3	18–65	0	0.7
4	33–80	-20.2	0.9
5	62–100	10	-1.6

TABLE II: SPDFs of birth labels

Birth	Mean	Covariance
$\mathcal{N}(\mathbf{x}^1, \mathbf{m}^1, \mathbf{P}^1)$	$[30, 0]^\top$	$\text{diag}\left(2^2, 0\right)$
$\mathcal{N}(\mathbf{x}^2, \mathbf{m}^2, \mathbf{P}^2)$	$[10, 0]^\top$	$\text{diag}\left(2^2, 0\right)$
$\mathcal{N}(\mathbf{x}^3, \mathbf{m}^3, \mathbf{P}^3)$	$[0, 0]^\top$	$\text{diag}\left(2^2, 0\right)$
$\mathcal{N}(\mathbf{x}^4, \mathbf{m}^4, \mathbf{P}^4)$	$[-20, 0]^\top$	$\text{diag}\left(2^2, 0\right)$

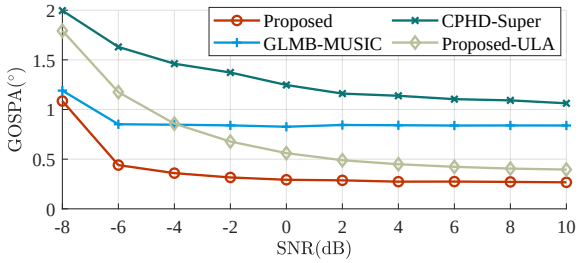

(a) Averaged GOSPA error versus SNR under $J = 200$ and $P = 100$

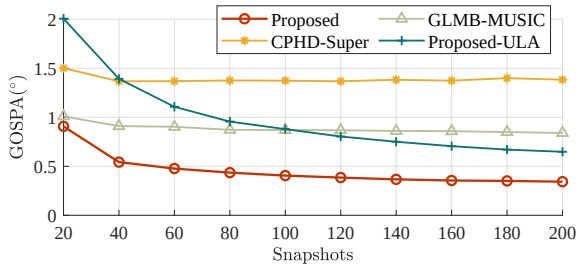

(b) Averaged GOSPA error versus snapshots under $\Gamma_{\text{SNR}} = -2\text{dB}$ and $P = 10$

Fig. 6: Averaged GOSPA error in the fixed source number scenario

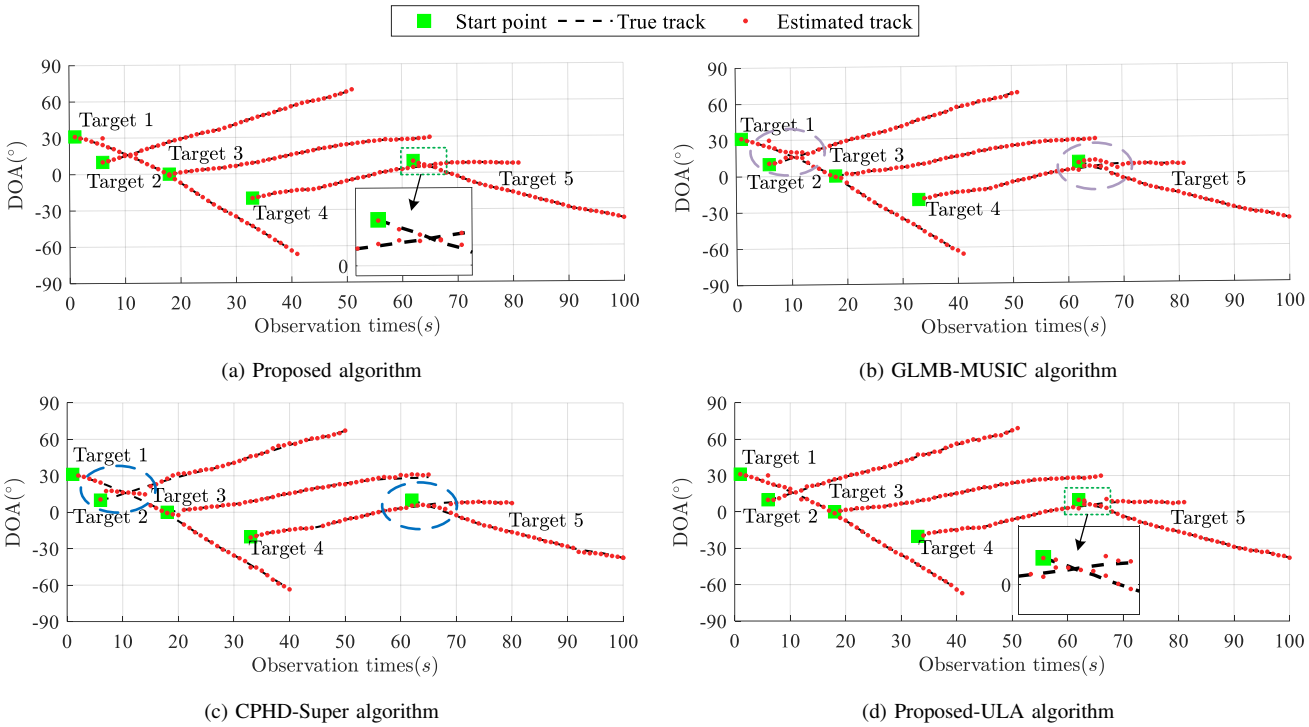

(a) Proposed algorithm

(b) GLMB-MUSIC algorithm

(c) CPHD-Super algorithm

(d) Proposed-ULA algorithm

Fig. 7: An example Monte Carlo trial under $\Gamma_{\text{SNR}} = -2\text{dB}, J = 200$ and $P = 100$. The green dashed box marks the region where two DOAs intersect, which is enlarged in the insets to compare tracking performance. The purple dashed circle in (b) highlights the crossing region where GLMB–MUSIC exhibits noticeable estimation bias despite correct detection, whereas the blue dashed circle in (c) indicates missed detection by CPHD–Super near the DOA intersection. In contrast, the proposed method in (a) achieves both accurate and precise tracking through the crossing region. Compared with the Proposed–ULA algorithm in (d), the proposed algorithm demonstrates higher robustness and improved estimation accuracy.

reveals the decomposition of the GOSPA metric into its principal components, i.e., the estimation error for the correctly associated DOA, missed and false detection. It can be observed that the GLMB–MUSIC exhibits significant DOA estimation errors for correctly associated sources in such challenging scenarios, as illustrated by the purple dashed circle in Fig. 7(b). This is because the MUSIC-based pseudo-likelihood deteriorates when the DOAs are closely spaced, as the signal subspaces of adjacent sources are no longer well separated. Finally, the average GOSPA metrics across various SNR and snapshot conditions are shown in Fig. 11, illustrating the performance gains achieved by the proposed algorithm over existing methods. As shown, the proposed algorithm consistently achieves lowest GOSPA errors across all SNR and snapshot conditions, maintaining superior performance even in low SNR and limited snapshot conditions, demonstrating strong robustness in complex dynamic environments.

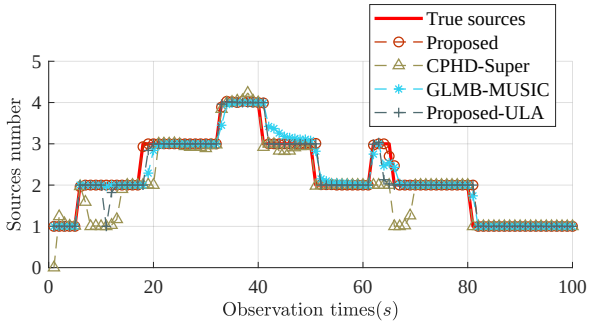

Fig. 8: Source number estimation under $\Gamma_{\text{SNR}} = -2\text{dB}, J = 200$ and $P = 100$

VI. Conclusions

In this paper, a robust generalized labeled multi-Bernoulli (GLMB) filter for multi-DOA tracking based on coprime arrays has been proposed. Unlike existing DOA tracking methods, this paper has derived a tensor model for coprime array receivers, the unique identifiability property of the canonical polyadic decomposition (CPD) has been leveraged to improve the association mapping strategy within the GLMB filter. Furthermore, a von Mises-Fisher (vMF) distribution has been proposed to model the association likelihood, and a uniform clutter density on the hypersphere has been defined, enabling the integration of the measurement model into a unified Bayesian random finite set (RFS) filtering framework.

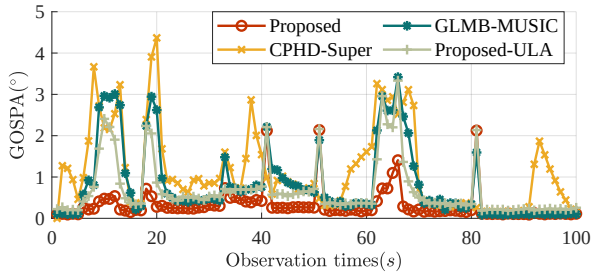

Fig. 9: GOSPA errors under $\Gamma_{\text{SNR}} = -2\text{dB}$, $J = 200$ and $P = 100$

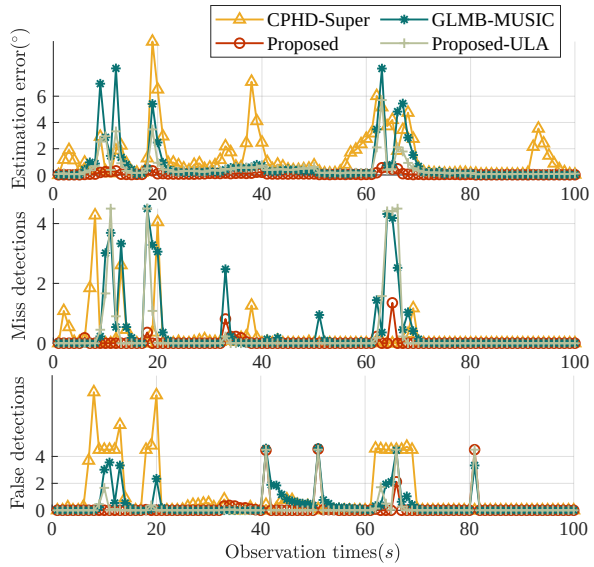

Fig. 10: DOA estimation error, missed and false detection errors under $\Gamma_{\text{SNR}} = -2\text{dB}$, $J = 200$ and $P = 100$

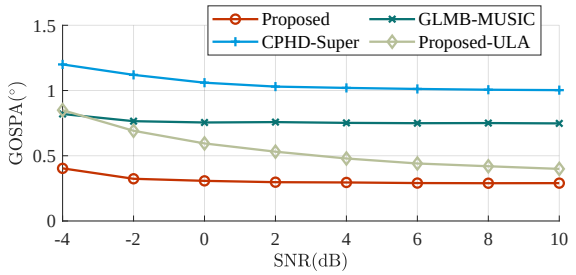

(a) Averaged GOSPA errors versus SNR under $J = 200$ and $P = 100$

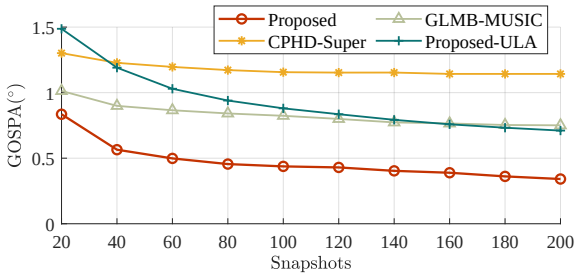

(b) Averaged GOSPA errors versus snapshots under $\Gamma_{\text{SNR}} = -2\text{dB}$ and $P = 10$

Fig. 11: Averaged GOSPA error in the time-varying source number scenario

Particle implementation has also been devised for the proposed algorithm. Finally, simulation experiments confirmed that the proposed algorithm achieves superior tracking performance compared to existing approaches. Future research could further develop the proposed algorithm to: 1) multi-DOA tracking for wideband sources; 2) consider array biases; 3) deteriorated scenarios involving, e.g., multipath, impulse noises, etc.

APPENDIX

A. Proof of proposition 1

For the γ-th segment ($\gamma = 1, \ldots, \nu$) of the sampled data, the virtual single-snapshot measurement vector in (8) generated from the sample covariance matrix can be represented by

$$\widetilde{\mathbf{r}}_k^{\gamma} = \widetilde{\mathbf{A}}_k \mathbf{b}_k^{\gamma} + \mathbf{u}_k^{\gamma}, \tag{56}$$

where $\mathbf{b}_k^{\gamma}$ denotes the source power vector of γ-th segment of the snapshots at time k, and the noise term $\mathbf{u}_k$ accounts for both the receiver measurement noise and the approximation error introduced by finite samples. In this paper, we assume that the power of each source (for $i = 1, \ldots, Q_k$) is independent and can be modeled as a slow-varying random walk process, expressed as

$$\sigma_{i,\gamma,k}^2 = \sigma_{i,\gamma-1,k}^2 + \epsilon_{i,\gamma,k}, \tag{57}$$

where $\epsilon_{i,\gamma,k}$ is a zero-mean Gaussian perturbation with a small covariance σ_{ϵ}^2 preventing the power from becoming negative. Based on this assumption, the source power vector in each segment is modeled as a Gaussian random vector

$$\mathbf{b}_k^{\gamma} \sim \mathcal{N}(\overline{\mathbf{b}}_k^{\gamma}, \mathbf{D}_k^{\gamma}),$$

where the mean vector $\overline{\mathbf{b}}_k^{\gamma} = [\sigma_{1,\gamma,k}^2, \cdots, \sigma_{Q_k,\gamma,k}^2]^{\top}$ and the covariance matrix is

$$\mathbf{D}_k^{\gamma} = \text{diag}\left[\sigma_{1,\gamma,k}^4, \ldots, \sigma_{Q_k,\gamma,k}^4\right] + \sigma_{\epsilon}^2 \mathbf{I}_{Q_k}.$$

Then the expected covariance matrix $\mathbb{E}\left(\mathbf{r}_k^{\gamma}(\mathbf{r}_k^{\gamma})^H\right)$ of the virtual single-snapshot vector is computed by

$$\begin{aligned}
\mathbb{E}\left(\mathbf{r}_k^{\gamma}(\mathbf{r}_k^{\gamma})^H\right) &= \mathbb{E}\left((\widetilde{\mathbf{A}}_k \mathbf{b}_k^{\gamma} + \mathbf{u}_k^{\gamma})(\widetilde{\mathbf{A}}_k \mathbf{b}_k^{\gamma} + \mathbf{u}_k^{\gamma})^H\right) \\
&= \widetilde{\mathbf{A}}_k \mathbf{D}_k^{\gamma} \widetilde{\mathbf{A}}_k^H + \mathbb{E}(2\widetilde{\mathbf{A}}_{\mathbf{k}} \mathbf{b}_k^{\gamma}(\mathbf{u}_k^{\gamma})^H) + \mathbb{E}(\mathbf{u}_k^{\gamma}(\mathbf{u}_k^{\gamma})^H) \\
&\triangleq \widetilde{\mathbf{A}}_k \mathbf{D}_k^{\gamma} \widetilde{\mathbf{A}}_k^H + \mathbf{U}_k^{\gamma},
\end{aligned} \tag{58}$$

where $\mathbf{U}_k^{\gamma} = \mathbb{E}(2\widetilde{\mathbf{A}}_{\mathbf{k}} \mathbf{b}_k^{\gamma}(\mathbf{u}_k^{\gamma})^H) + \mathbb{E}(\mathbf{u}_k^{\gamma}(\mathbf{u}_k^{\gamma})^H)$ can be seen as noise term since it is relatively small compared to the main term $\widetilde{\mathbf{A}}_k \mathbf{D}_k^{\gamma} \widetilde{\mathbf{A}}_k^H$.

As a result, the spatially smoothed covariance matrix in (9) can be seen as a finite-sample approximation of the expected covariance matrix (58), thus the smoothed covariance matrix of each segment sample data can be represented as

$$\widetilde{\mathbf{R}}_k^{\gamma} = \frac{1}{M} \sum_{j=1}^{M} \widetilde{\mathbf{r}}_{j,k}^{\gamma} (\widetilde{\mathbf{r}}_{j,k}^{\gamma})^H \approx \overline{\mathbf{A}}_k \mathbf{D}_k^{\gamma} \overline{\mathbf{A}}_k^H + \widetilde{\mathbf{U}}_k^{\gamma}, \tag{59}$$

where the virtual array manifold after spatial smoothing is defined as $\overline{\mathbf{A}}_k \triangleq [\overline{\mathbf{a}}(\theta_{1,k}), \cdots, \overline{\mathbf{a}}(\theta_{i,k}), \cdots, \overline{\mathbf{a}}(\theta_{Q_k,k})]$ with $\overline{\mathbf{a}}(\theta_{i,k})$ defined in (30), and $\widetilde{\mathbf{U}}_k^{\gamma}$ denotes the error term since M is finite. By leveraging the fact that $\mathbf{D}_k^{\gamma}$ is diagonal, the vectorization of (59) simplifies to

$$\begin{aligned}\mathrm{vec}(\widetilde{\mathbf{R}}_k^{\gamma}) &= \sum_{i=1}^{Q_k} \sigma_{i,\gamma,k}^4 \,\mathrm{vec}\big(\overline{\mathbf{a}}(\theta_{i,k})\overline{\mathbf{a}}(\theta_{i,k})^H\big) + \mathrm{vec}(\widetilde{\mathbf{U}}_k^{\gamma}) \\ &= \sum_{i=1}^{Q_k} \sigma_{i,\gamma,k}^4 \left(\overline{\mathbf{a}}^*(\theta_{i,k}) \otimes \overline{\mathbf{a}}(\theta_{i,k})\right) + \mathrm{vec}(\widetilde{\mathbf{U}}_k^{\gamma}) \\ &= \left(\overline{\mathbf{A}}_k^* \odot \overline{\mathbf{A}}_k\right) \mathbf{d}_k^{\gamma} + \mathrm{vec}(\widetilde{\mathbf{U}}_k^{\gamma}), \end{aligned} \tag{60}$$

where $\otimes$ denotes the Kronecker product, and vector $\mathbf{d}_k^{\gamma}$ is defined as:

$$\mathbf{d}_k^{\gamma} = [\sigma_{1,\gamma,k}^4, \ldots, \sigma_{Q_k,\gamma,k}^4]^T, \tag{61}$$

which contains the diagonal entries of $\mathbf{D}_k^{\gamma}$. By stacking all ν vectors defined in (60) as a matrix, we have

$$\begin{aligned}\mathbf{R}_{(3)} &\triangleq \left[\mathrm{vec}(\widetilde{\mathbf{R}}_k^1), \cdots, \mathrm{vec}(\widetilde{\mathbf{R}}_k^{\nu})\right] \\ &= \left(\overline{\mathbf{A}}_k^* \odot \overline{\mathbf{A}}_k\right) \overline{\mathbf{D}}_k^{\top} + \mathbf{U}_{(3)}, \end{aligned} \tag{62}$$

where $\overline{\mathbf{D}}_k \triangleq [\overline{\mathbf{d}}_k^1, \cdots, \overline{\mathbf{d}}_k^{Q_k}] = [\mathbf{d}_k^1, \cdots, \mathbf{d}_k^{\nu}]^{\top}$, $\mathbf{U}_{(3)} \triangleq [\mathrm{vec}(\widetilde{\mathbf{U}}_k^1), \cdots, \mathrm{vec}(\widetilde{\mathbf{U}}_k^{\nu})]$. It can be seen that this matrix corresponds to the mode-3 unfolding of a third-order tensor admitting CPD, as defined in (27).

As a result, if stacking ν smoothed covariance matrices along the third dimension, i.e., $\boldsymbol{\mathcal{R}}_k(:,:,\gamma) = \widetilde{\mathbf{R}}_k^{\gamma}, \gamma = 1, \cdots, \nu$, then the resulting multi-dimensional array can be regarded as a tensor admitting CPD, given by

$$\begin{aligned}\boldsymbol{\mathcal{R}}_k &\triangleq [\![\overline{\mathbf{A}}_k^*, \overline{\mathbf{A}}_k, \overline{\mathbf{D}}_k]\!] + \boldsymbol{\mathcal{U}}_k \\ &= \sum_{i=1}^{Q_k} \overline{\mathbf{a}}^*(\theta_{i,k}) \circ \overline{\mathbf{a}}(\theta_{i,k}) \circ \overline{\mathbf{d}}_k^i + \boldsymbol{\mathcal{U}}_k. \end{aligned} \tag{63}$$

This result is consistent with (22), and thus Proposition 1 has been proven.

■

REFERENCES

[1] X. Song, G. Ding, Y. Xu, H. Wang, J. Gu, and Y. Liu, "Cooperative sensing of non-cooperative beam signals," *IEEE Trans. Cogn. Commun. Netw.*, vol. 10, no. 3, pp. 807–818, 2023.

[2] S. E. Sorkhabi and K. Rambabu, "Multi-target DOA estimation with mmwave MIMO radar using limited number of sensors," *IEEE Trans. Veh. Technol.*, early access, 2025, doi: 10.1109/TVT.2025.3563443.

[3] A.-A. Saucan, T. Chonavel, C. Sintes, and J.-M. Le Caillec, "CPHD-DOA tracking of multiple extended sonar targets in impulsive environments," *IEEE Trans. Signal Process.*, vol. 64, no. 5, pp. 1147–1160, 2015.

[4] J. Wang, H. Xu, G. J. Leus, and G. A. Vandenbosch, "Experimental assessment of the coarray concept for DOA estimation in wireless communications," *IEEE Trans. Antennas Propag.*, vol. 66, no. 6, pp. 3064–3075, 2018.

[5] A. Alexandridis and A. Mouchtaris, "Multiple sound source location estimation in wireless acoustic sensor networks using DOA estimates: The data-association problem," *IEEE/ACM Trans. Audio, Speech, Lang. Process.*, vol. 26, no. 2, pp. 342–356, 2017.

[6] R. Schmidt, "Multiple emitter location and signal parameter estimation," *IEEE Trans. Antennas Propag.*, vol. 34, no. 3, pp. 276–280, 1986.

[7] R. Roy and T. Kailath, "ESPRIT-estimation of signal parameters via rotational invariance techniques," *IEEE Trans. Acoust., Speech, Signal Process.*, vol. 37, no. 7, pp. 984–995, 1989.

[8] D. L. Donoho, "Compressed sensing," *IEEE Trans. Inf. Theory*, vol. 52, no. 4, pp. 1289–1306, 2006.

[9] D. Malioutov, M. Cetin, and A. S. Willsky, "A sparse signal reconstruction perspective for source localization with sensor arrays," *IEEE Trans. Signal Process.*, vol. 53, no. 8, pp. 3010–3022, 2005.

[10] B. Lin, J. Liu, M. Xie, and J. Zhu, "Direction-of-arrival tracking via low-rank plus sparse matrix decomposition," *IEEE Antennas Wireless Propag. Lett.*, vol. 14, pp. 1302–1305, 2015.

[11] A. Das, "A Bayesian sparse-plus-low-rank matrix decomposition method for direction-of-arrival tracking," *IEEE Sens. J.*, vol. 17, no. 15, pp. 4894–4902, 2017.

[12] Z. Zheng, Y. Huang, W.-Q. Wang, and H. C. So, "Spatial smoothing PAST algorithm for DOA tracking using difference coarray," *IEEE Signal Process. Lett.*, vol. 26, no. 11, pp. 1623–1627, 2019.

[13] F. Dong, L. Xu, and X. Li, "Particle filter algorithm for DOA tracking using co-prime array," *IEEE Commun. Lett.*, vol. 24, no. 11, pp. 2493–2497, 2020.

[14] J. Cao, M. You, D. Li, X. Zhang, and F. Zhou, "Multi-source DOA tracking with an adaptive superposition model for sparse array," *Signal Process.*, vol. 230, p. 109877, 2025.

[15] N. Chen, P. Wei, L. Gao, W. Li, L. Liu, and H. Zhang, "Robust tracking of multiple targets subspace based on distributed array networks," *IEEE Trans. Aerosp. Electron. Syst.*, vol. 59, no. 6, pp. 9758–9768, 2023.

[16] R. Mahler, *Statistical Multisource-Multitarget Information Fusion*. Norwood, MA, USA: Artech House, 2007.

[17] R. P. Mahler, "Multitarget Bayes filtering via first-order multitarget moments," *IEEE Trans. Aerosp. Electron. Syst.*, vol. 39, no. 4, pp. 1152–1178, 2003.

[18] R. Mahler, "PHD filters of higher order in target number," *IEEE Trans. Aerosp. Electron. Syst.*, vol. 43, no. 4, pp. 1523–1543, 2007.

[19] B.-T. Vo, B.-N. Vo, and A. Cantoni, "The cardinality balanced multi-target multi-Bernoulli filter and its implementations," *IEEE Trans. Signal Process.*, vol. 57, no. 2, pp. 409–423, 2008.

[20] Y. Xia, K. Granström, L. Svensson, M. Fatemi, Á. F. García-Fernández, and J. L. Williams, "Poisson multi-Bernoulli approximations for multiple extended object filtering," *IEEE Trans. Aerosp. Electron. Syst.*, vol. 58, no. 2, pp. 890–906, 2021.

[21] S. Zhao, H. Zhang, L. Gao, M. You, W. Li, and P. Wei, "PMBM-based multi-target tracking under measurement merging," *Signal Process.*, vol. 225, p. 109610, 2024.

[22] B.-T. Vo and B.-N. Vo, "Labeled random finite sets and multi-object conjugate priors," *IEEE Trans. Signal Process.*, vol. 61, no. 13, pp. 3460–3475, 2013.

[23] B.-N. Vo, B.-T. Vo, and D. Phung, "Labeled random finite sets and the Bayes multi-target tracking filter," *IEEE Trans. Signal Process.*, vol. 62, no. 24, pp. 6554–6567, 2014.

[24] Y. Chen, L. Gao, L. Chisci, P. Wei, H. Zhang, and A. Farina, "Direct multi-emitter tracking based on the generalized labeled multi-Bernoulli filter," *IEEE Trans. Signal Process.*, early access, 2025.

[25] S. Reuter, B.-T. Vo, B.-N. Vo, and K. Dietmayer, "The labeled multi-Bernoulli filter," *IEEE Trans. Signal Process.*, vol. 62, no. 12, pp. 3246–3260, 2014.

[26] R. Mahler, "CPHD filters for superpositional sensors," in *Proc. SPIE Signal and Data Process. Small Targets (SDPST)*, vol. 7445. SPIE, 2009, pp. 150–161.

[27] D. Hauschildt, "Gaussian mixture implementation of the cardinalized probability hypothesis density filter for superpositional sensors," in *Proc. Int. Conf. Indoor Positioning Indoor Navigation (IPIN)*. IEEE, 2011, pp. 1–8.

[28] S. Nannuru, M. Coates, and R. Mahler, "Computationally-tractable approximate PHD and CPHD filters for superpositional sensors," *IEEE J. Sel. Topics Signal Process.*, vol. 7, no. 3, pp. 410–420, 2013.

[29] F. Thouin, S. Nannuru, and M. Coates, "Multi-target tracking for measurement models with additive contributions," in *Proc. Int. Conf. Inf. Fusion (Fusion)*. IEEE, 2011, pp. 1–8.

[30] H. Zhang, W. Luo, X. Zhou, H. Mu, L. Gao, and X. Wang, "A robust trajectory multi-Bernoulli filter for superpositional sensors," *Electronics*, vol. 13, no. 20, p. 4001, 2024.

[31] F. Papi, B.-N. Vo, B.-T. Vo, C. Fantacci, and M. Beard, "Generalized labeled multi-Bernoulli approximation of multi-object densities," *IEEE Trans. Signal Process.*, vol. 63, no. 20, pp. 5487–5497, 2015.

[32] A.-A. Saucan, Y. Li, and M. Coates, "Particle flow superpositional GLMB filter," in *Proc. SPIE Signal Process., Sensor/Information Fusion, and Target Recognition XXVI*, vol. 10200. SPIE, 2017, pp. 116–127.

[33] R. Mahler, "A fast labeled multi-Bernoulli filter for superpositional sensors," in *Proc. SPIE Signal Process., Sensor/Information Fusion, and Target Recognition XXVII*, vol. 10646. SPIE, 2018, pp. 113–124.

[34] G. Li, P. Wei, Y. Li, L. Gao, and H. Zhang, "A robust fast LMB filter for superpositional sensors," *Signal Process.*, vol. 174, p. 107606, 2020.

[35] A. Masnadi-Shirazi and B. D. Rao, "A covariance-based superpositional CPHD filter for multisource DOA tracking," *IEEE Trans. Signal Process.*, vol. 66, no. 2, pp. 309–323, 2017.

[36] J. Zhao, R. Gui, and X. Dong, "A new measurement association mapping strategy for DOA tracking," *Digit. Signal Process.*, vol. 118, p. 103228, 2021.

[37] J. Zhao, X. Dong, M. Sun, X. Zhang, and Y. Wang, "WSN-PHD: A novel moving target DOA tracking algorithm," *IEEE Internet of Things Journal*, 2025.

[38] S. Qin, Y. D. Zhang, and M. G. Amin, "Generalized coprime array configurations for direction-of-arrival estimation," *IEEE Trans. Signal Process.*, vol. 63, no. 6, pp. 1377–1390, 2015.

[39] J. Zhao, R. Gui, and X. Dong, "PHD filtering for multi-source DOA tracking with extended co-prime array: an improved MUSIC pseudo-likelihood," *IEEE Commun. Lett.*, vol. 25, no. 10, pp. 3267–3271, 2021.

[40] X. Dong, J. Zhao, M. Sun, X. Zhang, and Y. Wang, "A modified δ-generalized labeled multi-Bernoulli filtering for multi-source DOA tracking with coprime array," *IEEE Trans. Wireless Commun.*, vol. 22, no. 12, pp. 9424–9437, 2023.

[41] J. Pan, M. Sun, Y. Wang, and X. Zhang, "An enhanced spatial smoothing technique with ESPRIT algorithm for direction of arrival estimation in coherent scenarios," *IEEE Trans. Signal Process.*, vol. 68, pp. 3635–3643, 2020.

[42] R. P. Mahler, *Advances in Statistical Multisource-Multitarget Information Fusion*. Norwood, MA, USA: Artech House, 2014.

[43] N. D. Sidiropoulos, L. De Lathauwer, X. Fu, K. Huang, E. E. Papalexakis, and C. Faloutsos, "Tensor decomposition for signal processing and machine learning," *IEEE Trans. Signal Process.*, vol. 65, no. 13, pp. 3551–3582, 2017.

[44] P. Comon, X. Luciani, and A. L. De Almeida, "Tensor decompositions, alternating least squares and other tales," *J. Chemometrics*, vol. 23, no. 7–8, pp. 393–405, 2009.

[45] K. Huang, N. D. Sidiropoulos, and A. P. Liavas, "A flexible and efficient algorithmic framework for constrained matrix and tensor factorization," *IEEE Trans. Signal Process.*, vol. 64, no. 19, pp. 5052–5065, 2016.

[46] M. Sørensen and L. De Lathauwer, "Blind signal separation via tensor decomposition with Vandermonde factor: Canonical polyadic decomposition," *IEEE Trans. Signal Process.*, vol. 61, no. 22, pp. 5507–5519, 2013.

[47] M. Wax and T. Kailath, "Detection of signals by information theoretic criteria," *IEEE Trans. Acoust., Speech, Signal Process.*, vol. 33, no. 2, pp. 387–392, 2003.

[48] C.-T. Do, T. T. D. Nguyen, and H. Van Nguyen, "Robust multi-sensor generalized labeled multi-Bernoulli filter," *Signal Process.*, vol. 192, p. 108368, 2022.

[49] R. P. Mahler, B.-T. Vo, and B.-N. Vo, "CPHD filtering with unknown clutter rate and detection profile," *IEEE Trans. Signal Process.*, vol. 59, no. 8, pp. 3497–3513, 2011.

[50] H. W. Kuhn, "The Hungarian method for the assignment problem," *Naval Res. Logist. Q.*, vol. 2, no. 1–2, pp. 83–97, 1955.

[51] M. L. Miller, H. S. Stone, and I. J. Cox, "Optimizing Murty's ranked assignment method," *IEEE Trans. Aerosp. Electron. Syst.*, vol. 33, no. 3, pp. 851–862, Jul. 1997.

[52] A. S. Rahmathullah, Á. F. García-Fernández, and L. Svensson, "Generalized optimal sub-pattern assignment metric," in *Proc. Int. Conf. Inf. Fusion (Fusion)*. IEEE, 2017, pp. 1–8.